
DISENTANGLING REGIONAL IMPACTS OF JOINT TELECONNECTIONS USING CAUSAL REPRESENTATION LEARNING

Fiona R. Spuler
Department of Meteorology
University of Reading, Reading, UK
f.r.spuler@pgr.reading.ac.uk

Marlene Kretschmer
Leipzig Institute for Meteorology
University of Leipzig,
Leipzig, Germany

Magdalena Alonso Balmaseda
European Centre for Medium-Range
Weather Forecasts
Reading, UK

Masilin Gudoshava
IGAD Climate Prediction and Applications Centre
Nairobi, Kenya

Theodore G. Shepherd
Department of Meteorology,
University of Reading
Reading, UK

Keywords: causal representation learning, teleconnections, seasonal predictability, variational autoencoders, regional impacts

Abstract: Understanding teleconnections of large-scale modes of climate variability is relevant for seasonal predictability and support a dynamical understanding of climatic changes. While numerical model experiments are the most common approach for investigating counterfactual climate responses, their conclusions are subject to model biases. Data-driven approaches offer a complementary perspective. Deep learning can extract reduced-dimensional patterns but usually lacks causal interpretability, while causal methods can disentangle signals in the presence of confounding yet are typically based on simple indices. Treating dimensionality reduction and causal inference separately thereby risks losing the teleconnection signal of interest. This paper introduces DAG-VAE, a causal representation learning approach that embeds a physics-informed directed acyclic graph in the latent space of a variational autoencoder. Combining deep learning with causal inference, the method jointly learns nonlinear reduced representations of large-scale modes of variability and their causal interactions. We apply DAG-VAE to disentangle the influences of the Pacific and Indian Oceans on the short rains over the Greater Horn of Africa. Trained on seasonal hindcasts, the method identifies dynamically meaningful representations and recovers spatial response patterns consistent with SST-replacement experiments. Trained on reanalysis data, DAG-VAE identifies a different response pattern to direct influence of the tropical Pacific, highlighting potential model biases and the value of DAG-VAE as a complementary, data-driven approach for estimating spatial causal response patterns from observations. Finally, we demonstrate the ability of the method to generate data-driven counterfactuals of extreme short rain seasons, with potential applications for forecast-based early action and scenario planning.

Significance statement: Investigating how large-scale climate variability affects regional rainfall is important for improving seasonal forecasts and the dynamical understanding of future climate change. Numerical model experiments are commonly used to infer causal teleconnections, but are subject to model biases. Data-driven methods can be trained on observations, yet they often struggle to disentangle causal pathways, especially when spatial patterns are complex and nonlinear. Here, we address this problem by developing a data-driven method that jointly learns low-dimensional representations of climate variability and their causal links, combining causal inference with deep learning. Applied to the Greater Horn of Africa, the method successfully disentangles teleconnection patterns from the Indian and Pacific Oceans and enables the generation counterfactual simulations of plausible extreme short-rain seasons.

1 Introduction

Large-scale modes of variability in the climate system and their teleconnections provide important sources of predictability at subseasonal to seasonal timescales and a dynamical foundation for understanding near-term to end-of-century climate change [Mariotti et al., 2020, Liné et al., 2024, Mindlin et al., 2025]. However, developing

a robust dynamical understanding of teleconnections and disentangling their joint effects on surface-level extremes remains challenging due to model biases in representing teleconnections [Stan et al., 2022, Gler et al., 2025] and the relatively short observational record, background-state dependence and non-stationarity of teleconnections, as well as the difficulty in identifying causal effects in high-dimensional spatiotemporal data [Runge et al., 2019b, Saggiaro et al., 2020, Wainwright et al., 2019].

Over the Greater Horn of Africa (GHA), the seasonal movement of the Intertropical Convergence Zone modulates rainfall variability, leading to a spatially varying bimodal climatology of “long rains” (March-May) and “short rains” (October-December) [Palmer et al., 2023, Nicholson, 2017]. The short rain season, while more predictable, exhibits strong interannual variability and has been associated with both droughts and heavy rainfall, causing severe impacts on lives and livelihoods in recent years [Gudoshava et al., 2024, Nana et al., 2025a].

At seasonal timescales, the intensity and predictability of the short rains is influenced by teleconnections from the tropical Pacific and Indian Ocean, in particular the El Niño Southern Oscillation (ENSO) and Indian Ocean Dipole (IOD) through the modulation of the Indian Ocean Walker circulation [Gudoshava et al., 2022, Black et al., 2003, Black, 2005, Kolstad and MacLeod, 2022, Palmer et al., 2023, Tefera et al., 2025]. ENSO is a coupled ocean–atmosphere phenomenon in the tropical Pacific and a leading mode of interannual climate variability globally [Timmermann et al., 2018], while the IOD describes a dipole pattern of sea surface temperature anomalies in the Indian Ocean which peaks between September and November [Saji et al., 1999, Webster et al., 1999]. El Niño and positive IOD conditions typically lead to anomalous subsidence over the eastern Indian Ocean, a reversal of the climatological westerlies, and enhanced convection and precipitation over the GHA, with the reverse effect observed during La Niña and negative IOD conditions [Palmer et al., 2023, Zheng et al., 2025].

Although ENSO is considered to be one of the processes influencing the IOD, the IOD can also occur independently [Wainwright et al., 2021, Wang et al., 2024a, Cai et al., 2019, Sun et al., 2015]. Therefore, disentangling whether the seasonal teleconnection from the two ocean basins is primarily mediated via the Indian Ocean, or whether the tropical Pacific can exert a direct influence, independent of the IOD, remains challenging. Understanding this direct influence has important consequences for applications such as early warnings and anticipatory action. For instance, during the 2015 El Niño, flood preparedness action was taken in the humanitarian sector in Somalia and Kenya, based on past anomalies associated with strong El Niño events [Tozier de la Poterie et al., 2018]. However, the short rains that year were less intense and more spatially variable than forecast, in part due to weaker than forecast sea surface temperature (SST) anomalies over the Indian Ocean [MacLeod and Caminade, 2019]. This highlights the importance of better understanding whether the precipitation response to El Niño is entirely mediated by the in-phase occurrence of a positive IOD, or whether a direct effect from the tropical Pacific exists.

The causal effects of remote SST anomalies on regional precipitation have traditionally been explored using model experiments, such as SST-replacement experiments [Richter et al., 2025]. Early studies found that the region-wide wetting or drying anomaly over the GHA is primarily mediated via the Indian Ocean, rather than via a direct pathway from the tropical Pacific [Latif et al., 1999, Goddard and Graham, 1999]. However, SST replacement experiments conducted by MacLeod et al. [2021] showed that while the primary pathway leading to an overall wetting or drying response is indeed mediated by the Indian Ocean, there is an additional direct pathway from the tropical Pacific to the GHA short rains that exhibits a different spatial precipitation response pattern: instead of an overall wetting or drying over the region, the authors argue that in the model considered, the direct effect of ENSO leads to a weaker dipole pattern response with a wetting off the coast of the GHA and a drying further inland in response to El Niño, and the opposite for La Niña.

While model experiments enable conditioning on specific states of a remote driver, their findings are necessarily subject to model errors and biases. Seasonal forecast systems as well as climate projections tend to underestimate the positive skewness of both ENSO and the IOD, exhibit mean state biases in the IOD that influence climatological precipitation over East Africa, and show an emerging El Niño-like response to anthropogenic emissions not found in observations [Gler et al., 2025, Wang et al., 2024a, Timmermann et al., 2018, Beverley et al., 2024, Hirons and Turner, 2018]. The relationship between ENSO and IOD has also been hypothesised to be too strong in some forecasting systems [MacLeod and Caminade, 2019]. Furthermore, depending on the research question, the unphysical constraint imposed by a hard SST boundary condition that does not allow for atmosphere-ocean feedbacks, leading to unrealistic heat sources or sinks, poses limitations on the findings [O’Reilly et al., 2023, Barsugli and Battisti, 1998]. Numerical model experiments are also computationally expensive, which prevents their use in real time, limiting the ability to understand

and communicate the predicted seasonal forecast anomaly effectively, in turn affecting decision-making based on early warnings.

These limitations call into question the extent to which model-based causal inferences hold in the observed climate system and motivate the development of complementary data-driven approaches. Recent advances in causality research have spurred the development of new data-driven methods for investigating teleconnections in a causal framework [Kretschmer et al., 2016, 2020, Runge et al., 2019a, Saggioro et al., 2024, Di Capua et al., 2020], based on the mathematical formalisation and representation of causal mechanisms as directed acyclic graphs [Pearl, 2009, Peters et al., 2017]. These methods are based on either discovering causal graphs from time series data by ruling out non-causal relations using constraint-based [Runge et al., 2014, 2019b] or score-based methods [Peters et al., 2017], or assuming the causal graph based on physical hypotheses [Kretschmer et al., 2021].

However, existing causal approaches often rely on predefined indices as representations of the modes of variability studied - such as the Niño3.4 for ENSO or the Dipole Mode Index (DMI) for the IOD [Kolstad and MacLeod, 2022]. While such indices can provide useful standardization for the scientific community, they risk averaging out the signal of interest and obscuring physically meaningful patterns. In particular, both ENSO and IOD exhibit what is known as diversity, namely that different SST anomaly patterns with different surface-level impacts, drivers, and responses to global warming can be associated with the same index [Capotondi et al., 2015, Guo et al., 2015, Fischer et al., 2005, Du et al., 2013, Johnson and Wichern, 2013, Guillaume-Castel et al., Zhang et al., 2024, Fang et al., 2024]. These diverse SST patterns have also been shown to influence their teleconnections to the short rains [Wang et al., 2024a, Tozuka et al., 2016, Liu et al., 2017, MacLeod et al., 2021]. On the other hand, common dimensionality reduction approaches for representing large-scale modes, such as Empirical Orthogonal Function (EOF) analysis (also called principal component analysis; PCA), assume linearity, are not necessarily physically interpretable [Dommenges and Latif, 2002], and treat dimensionality reduction separately from causal inference [Saji et al., 1999, Wang et al., 2024a]. In the application studied in this paper, the precipitation dipole identified by MacLeod et al. [2021] could not be identified using the first principal component or regional average precipitation over the GHA used for example in Kolstad et al. [2021]. In addition, Kolstad et al. [2024] investigate the drivers of different spatial precipitation patterns over the GHA and highlight, along with Nicholson [2017], the need to go beyond the regional average of precipitation for better understanding drivers and predicting impacts.

Deep learning approaches, such as graph neural networks, on the other hand, also learn nonlinear latent representations. However, these are optimized for prediction rather than representation of the underlying dynamical processes and are not necessarily physically or causally interpretable. The emerging field of causal representation learning aims to address this limitation by jointly learning reduced representations of high-dimensional data and their causal structure [Scholkopf et al., 2021]. While the majority of papers in this field have focused on established applications in computer science such as computer vision, a few recent papers have proposed methods to investigate causal links in the climate system [Boussard et al., 2023, Wang et al., 2024b, Hickman et al., 2025]. These methods primarily work towards climate model emulation and make general assumptions about the structure of the latent space, such as the single parent structure assumed in Boussard et al. [2023], but do not easily incorporate existing knowledge about dynamical processes in the model structure.

In this work, building on these recent advances in causal representation learning, we propose a new data-driven method to jointly identify dimensionality-reduced representations of climatic processes alongside the causal effects of interacting teleconnections. Our proposed method, DAG-VAE, embeds a physics-informed directed acyclic graph (DAG) in the latent space of a variational autoencoder (VAE), harnessing the ability of generative deep learning methods to identify structure in high-dimensional fields through nonlinear dimensionality reduction. The design of the architecture builds on previous work by Spuler et al. [2024a, 2025] and Swaroop et al. [2023]. By combining causal inference with deep learning, the DAG-VAE method further enables the generation of data-driven counterfactuals in the climate system. We investigate the ability of this new approach to disentangle the joint influence of the tropical Pacific and Indian Ocean on the short rains over the GHA with the following objectives: 1) Learning interpretable reduced representations of large-scale modes of variability alongside their causal relations; 2) Estimating the spatial causal response patterns of precipitation to individual modes of variability in the causal graph; 3) Generating counterfactuals of seasonal precipitation based on the causally-related reduced representations.

Section 2 provides details of the data used to train the model. We then introduce the method, DAG-VAE, in Section 3 and contextualise it in the field of causal representation learning. Section 4 presents the results. We first apply the

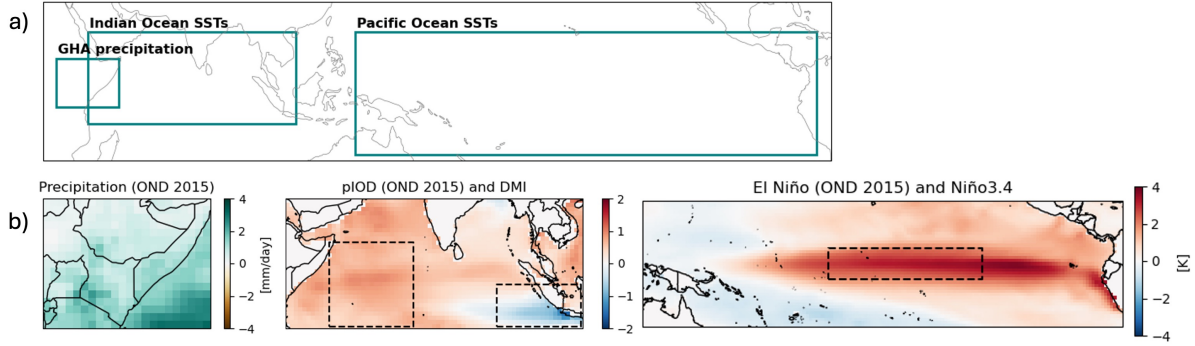


Figure 1: a) Illustration of the selected regions and variables used to study Greater Horn of Africa (GHA) precipitation, Indian Ocean (IO) and Pacific Ocean sea surface temperatures (SSTs). (b) Anomalies of precipitation over the GHA, SST patterns associated with a positive Indian Ocean Dipole and an El Niño season, showing October to December averages of the seasonal hindcast initialised in September 2015. The dashed black boxes indicate the regions used to compute the Dipole Mode Index and the Niño3.4 index.

method to seasonal hindcasts produced by ECMWF’s seasonal prediction system SEAS5 [Johnson et al., 2019]. This allows us to compare our results with the model experiments conducted by MacLeod et al. [2021] and to evaluate the robustness of the joint representations on a larger test set than would be available from reanalysis or observational data. We can thereby benchmark the data-driven approach to seasonal attribution presented in this paper to state-of-the-art methods based on model experiments. We then apply the method to reanalysis data - where replacement experiments could not be conducted - and compare the spatial causal effects estimated from the Pacific and Indian Ocean basins to the results found in the seasonal prediction model. In a final step, we generate counterfactual short rain seasons based on combinations of recent extreme drivers. We discuss these results and conclude in Section 5.

2 Data

We investigate SEAS5 seasonal hindcasts initialized retrospectively from ERA-Interim using the IFS CY43R1 on a TCo319 grid for the time period from 1981 to 2023 [Johnson et al., 2019]. We consider the short rains season (October - December) for the following variables and regions:

- SSTs in the tropical Pacific: (latitudes: $20^{\circ}S - 20^{\circ}N$; longitudes: $130^{\circ}E - 75^{\circ}W$);
- SSTs in the Indian Ocean: (latitudes: $10^{\circ}S - 20^{\circ}N$; longitudes: $40 - 110^{\circ}E$);
- Precipitation over the Greater Horn of Africa: (latitudes: $4.5^{\circ}S - 11.5^{\circ}N$; longitudes: $29.5 - 50.5^{\circ}E$).

Both monthly data and seasonal data are analysed in SEAS5, and lead times of 2-6 months are retained for verification months October-December. When analysing seasonal averages, this includes initialization dates from July-September; for individual months, this includes start dates from April-November. Forecast skill of SEAS5 for the short rains is discussed in Tefera et al. [2025], Nana et al. [2025b].

We investigate the sensitivity of results to using only September start dates and find no major qualitative differences in the results (not shown). Furthermore, the sensitivity to applying the method on monthly vs seasonal data was investigated and no qualitative differences were found in the average causal effect estimated, which is the focus of this paper. We choose to work with seasonal data to more closely match MacLeod et al. [2021] to facilitate comparison.

The SEAS5 hindcasts are pre-processed in the following way: The mean bias is removed by computing anomalies with respect to the verification month and lead time. Furthermore, we remove the average trend over the area, ensemble, lead time and verification month. We choose to remove the spatially averaged trend to retain pattern effects and their influence on rainfall. The sensitivity of the results to removing the trend, or removing the grid-point-wise trend, is analysed and no major difference in the causal response patterns estimated is found. In the Pacific, the mean estimate of the trend in seasonal hindcasts is found to be lead time dependent (see Appendix A), consistent with the findings of Mayer et al. [2025]. However, the uncertainty in the estimate of the trend is large compared to the lead time dependence of the mean estimate. We therefore choose to remove the trend averaged over lead times. Furthermore, we standardise the data prior to input

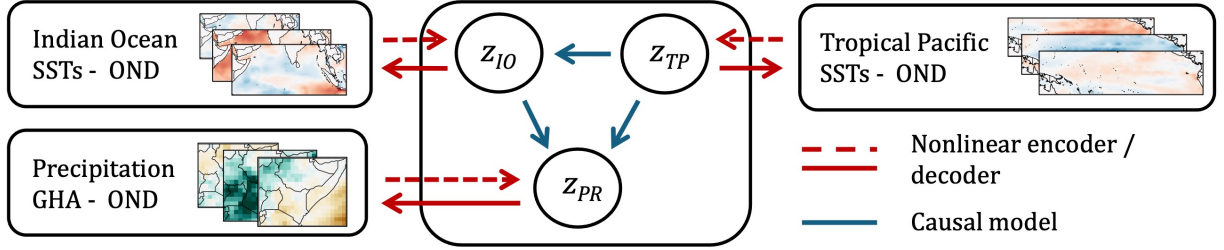


Figure 2: Illustration of the DAG-VAE method and architecture. z_{TP} , z_{IO} and z_{PR} refer to the low-dimensional representations identified by the model for the three high-dimensional input spaces: tropical Pacific SSTs, Indian Ocean SSTs and GHA precipitation. The red arrows refer to encoder and decoder neural networks that dimensionality-reduce the high-dimensional input space. The blue arrows refer to the directed acyclic graph (DAG) hypothesized in the latent space.

to the neural network. Since the grid-point-wise averages are already removed, we only divide by the average standard deviation of the entire field to retain the higher variability in some regions (e.g. the east Indian Ocean dipole region).

We fine-tune the architecture on ERA5 reanalysis data [Hersbach et al., 2020] from 1981-2023 for the same variables and regions as for SEAS5, whereby ERA5 uses the HadISST2.1.1.0 SST dataset as boundary condition. We regrid ERA5 data to match SEAS5 (1° resolution) and aggregate it from hourly data to 30-day averages, with data every 5 days used for training. The remaining pre-processing mirrors the SEAS5 pre-processing described above.

3 Method - DAG-VAE

We propose the Directed Acyclic Graph Variational Autoencoder (DAG-VAE) method which combines variational autoencoders for nonlinear dimensionality reduction with directed acyclic graphs for causal inference in a single architecture, illustrated in Figure 2. Variational autoencoders (VAEs) are a class of generative deep learning models that identify a probabilistic reduced representation of a high-dimensional input space [Kingma and Welling, 2013]. VAEs enable the generation of new samples from the probability distribution identified in the reduced (also called latent) space, and are trained using Bayesian variational inference, whereby a prior is set on the probability distribution of the latent space. In our application, this prior encodes a DAG between the latent distributions of coupled variational autoencoders. Each node of the DAG represents the latent representation of one of the variables - SSTs over the Indian and Pacific Oceans, and precipitation over the GHA - while each directed edge represents the hypothesized causal influence between variables. The DAG-VAE method builds on earlier work introduced by the authors in [Spuler et al., 2024a, 2025].

The causality of this model is based on dynamical understanding of the physical processes involved in the teleconnections studied [Kretschmer et al., 2021], as well as proofs for identifiability of the model presented by Lachapelle et al. [2022] and Shen et al. [2022]. Based on existing literature and understanding of dynamical processes discussed in Section 1, we assume a structural causal model in the latent space, shown in Figure 2. In particular, we assume that teleconnections from both the tropical Pacific and Indian Ocean are the primary teleconnections influencing the short rains on the timescales and lead times considered and that ENSO is the leading mode of variability on these timescales. Second, we assume that the selected variables, SST and precipitation anomalies, represent the physical processes underlying the teleconnection.

The field of causal representation learning was challenged early on by the result that unsupervised learning will not, in general, identify disentangled representations [Locatello et al., 2019] and that several different representations can lead to the same loss function - the 'true' causal relations are said to be non-identifiable in this case [Scholkopf et al., 2021]. Identifiability is defined as the uniqueness of the identified model parameters θ given an observed probability distribution P_θ ($P_\theta = P_{\tilde{\theta}} \Rightarrow \theta = \tilde{\theta}$). Research effort has since focused on finding strategies to ensure identifiability, often up to transformations such as permutations [Khemakhem et al., 2020, Lachapelle et al., 2022, Brouillard et al., 2024]. Shen et al. [2022] show that setting a structural causal model as a prior in the latent space ensures disentanglement of the causal factors conditional on the prior assumed. Furthermore, Lachapelle et al. [2022] show that if the target field (precipitation in our case) is affected sufficiently strongly by external

observed influences (ENSO and the IOD in our case), then identifiability up to certain transformations can be ensured by enforcing sparsity regularisation. Sufficiently strongly here means that the response to the external factors, called actions in Lachapelle et al. [2022], covers the full latent subspace that is causally influenced by that action.

Building on this research, the DAG-VAE method sets a structural causal model prior based on physical assumptions, and enforces sparsity both in this latent causal model by introducing a LASSO penalty (L1 norm), as well as in the number of latent dimensions in the reduced representations to ensure the disentanglement of the signals of interest in our representations. In this paper, the number of reduced dimensions was set to one for the tropical Pacific and Indian Ocean, and two for monthly precipitation over the GHA, as this was the minimal model needed to capture the dynamical processes analyzed. However, alternative versions with a higher number of latent dimensions (4-10) also produced qualitatively similar precipitation response patterns, as did versions that included independent noise dimensions for precipitation (not shown).

The DAG-VAE method jointly fits a nonlinear dimensionality reduction through encoder/decoder neural networks (red arrows in Figure 2) and a causal model between the latent representations z_{TP} , z_{IO} and z_{PR} (blue arrows in Figure 2), which are samples from probability distributions with Gaussian priors. This joint optimisation is conducted through the minimisation of the following modified loss function:

$$\begin{aligned} L_{DAG-VAE}(x_{TP}, x_{IO}, x_{PR}) = & \mathbb{E}_{q(z_{TP}|x_{TP})} \log p(x_{TP} | z_{TP}) - D_{KL}(q(z_{TP} | x_{TP}) || p(z_{TP})) \\ & + \mathbb{E}_{q(z_{IO}|x_{IO})} \log p(x_{IO} | z_{IO}) - D_{KL}(q(z_{IO} | x_{IO}) || p(z_{IO} | z_{TP})) \\ & + \mathbb{E}_{q(z_{PR}|x_{PR})} \log p(x_{PR} | z_{PR}) - D_{KL}(q(z_{PR} | x_{PR}) || p(z_{PR} | z_{IO}, z_{TP})) \end{aligned} \quad (1)$$

The loss function can be consistently derived from the graphical model shown in Appendix B, alongside a detailed description of the architecture and hyperparameters chosen. The first terms in each row represent the reconstruction loss terms for each of the input fields x_{TP} , x_{IO} and x_{PR} . The second terms in each row minimize the KL-divergences (denoted D_{KL}) - measures of the distance between two probability distributions - between the latent representation based on the input fields and the prediction of the latent representation based on the causal parents. The loss function thereby encodes the dual aim of the model, in identifying meaningful representations of the high-dimensional gridded input data, as well as informative and causally related signals.

We choose to model the causal relationships in the latent space using a linear model for a number of reasons, although implementing a nonlinear model would merely require adding an additional layer and activation function to the latent neural network. We assume that nonlinearities in the teleconnections can be captured through the nonlinear dimensionality reduction, enabling us to construct a linear model in the latent space which is sparser (less prone to overfitting) and for which the causal effect estimation is simpler. This is based on the intuition that the reduced representations themselves are affected by less noise (thus, are less prone to overfitting) than the relationships between the full representations. Furthermore, recent results suggest that the combination of nonlinear dimensionality reduction and linear relationships is the most successful when comparing the results of joint representation learning to other approaches [Brouillard et al., 2024].

In this version of the architecture, no time-lags are included in the model, although the method can, in principle, be fit for any chosen time-lag. The choice to not include time-lags here was made as the atmospheric response to the SSTs and resulting teleconnection to precipitation over the GHA is assumed to occur at timescales below one month, and is therefore 'instantaneous' when working with seasonal or monthly data. This assumption and choice is in line with current practices in SST replacement experiments such as MacLeod et al. [2021].

We compare our results against three baseline methods where appropriate. The first combines linear dimensionality reduction using Principal Component Analysis (PCA, also called EOF analysis in climate science) on the three input fields individually, retaining the same amount of latent dimensions as chosen for the DAG-VAE, with a subsequent linear prediction model. PCA, commonly referred to as EOF analysis in climate science, projects a higher-dimensional input space into a reduced space spanned by the orthogonal eigenvectors of the covariance matrix of the data [Jolliffe and Cadima, 2016]. As discussed in the introduction, PCA is a widely-used method in the study of teleconnections [Dommenget and Latif, 2002]. The second and third methods are based on established indices of ENSO and IOD, the Dipole Mode Index for the Indian Ocean and the Niño3.4 index for the Pacific, shown in Figure 1. In the first version (Indices v1), we use regionally averaged precipitation over the GHA to estimate the teleconnection, as, for example, in

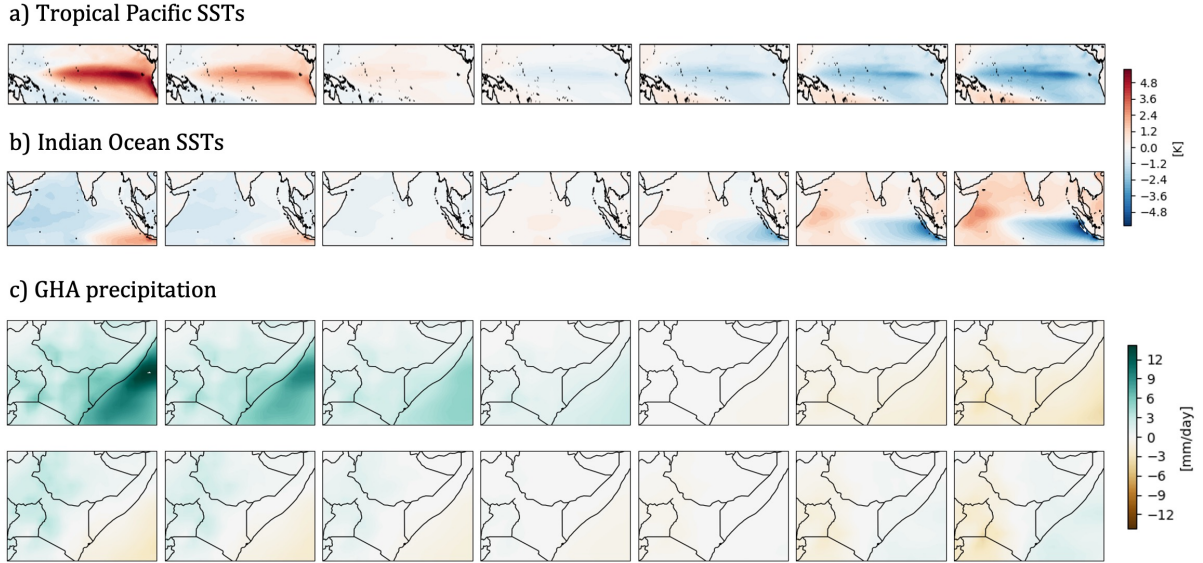


Figure 3: Illustration of the learned causal representations in SEAS5, shown through reconstructed samples of the latent dimensions z_{TP} , z_{IO} and $z_{PR1,2}$. The samples are created by first selecting equidistant samples from the means of the latent Gaussians, ranging from the minimum to the maximum value encountered in test set. Second, these samples are passed back through the decoder to reconstruct their original dimension.

Kolstad and MacLeod [2022]. In the second version (Indices v2), we use these two indices to fit a linear regression to precipitation at each grid point over the GHA.

4 Results

4.1 Identifying causal representations in seasonal hindcasts

We first evaluate the ability of the DAG-VAE to identify reduced and informative representations of the modes of variability when trained on seasonal hindcasts. To this end, we first visualize the information encoded in the latent space of the VAE by sampling from the reduced representations of each encoded variable. These samples are then passed through the decoder and thereby reconstructed to their original dimensions. Results are shown in Figure 3.

We find that the DAG-VAE identifies reduced representations z_{TP} and z_{IO} that capture SST patterns associated with the two main modes of variability in the two ocean basins during this season, ENSO and the IOD, seen in the decoded samples of the latent dimension representing the Tropical Pacific SSTs in Figure 3a, and the Indian Ocean SSTs in Figure 3b. This result shows that the DAG-VAE method is able to identify representations that are interpretable and physically meaningful.

Furthermore, the nonlinear dimensionality reduction in DAG-VAE is able to capture known asymmetries of both the ENSO and IOD patterns: El Niño anomalies are slightly more intense and reach further east than the La Niña anomalies, which are located more in the central Pacific; positive IOD events are also associated with more intense SST anomalies, in particular the negative anomalies in the east Indian Ocean which also extend spatially further west than the corresponding positive anomalies in the negative IOD phase. The detection of these asymmetric patterns would not be possible with a linear dimensionality reduction method such as PCA.

In terms of the reduced representations of precipitation over the GHA, we find that the first dimension, z_{PR1} , shown in the first row of Figure 3c, represents an overall wetting/drying over the entire region. Again, there is a slight asymmetry captured by the nonlinear dimensionality reduction: while the drying signal is relatively uniform spatially, the wetting signal is slightly stronger off the coast of the GHA, reflecting a known bias in the seasonal forecasting system. The

Table 1: Evaluation of key characteristics of the latent dimensions. The numbers in brackets refer to the metric evaluated only over the test set. The number after the \pm refers to the standard deviation.

a) Reconstruction loss - Root Mean Squared Error (RMSE)

	Tropical Ocean SSTs	Indian Ocean SSTs	GHA precipitation
DAG-VAE	0.32 ± 0.18 (0.33 ± 0.18)	0.51 ± 0.41 (0.52 ± 0.42)	0.31 ± 0.17 (0.32 ± 0.18)
PCA	0.36 ± 0.20	0.64 ± 0.48	0.36 ± 0.21

b) Predictive performance - GHA precipitation

	DAG-VAE	PCA	Indices v1	Indices v2
Anomaly Correlation Coefficient	0.68 (0.65)	0.51 (0.50)	0.39 (0.38)	0.50 (0.48)
R^2 total precipitation	0.58 (0.55)	0.43 (0.43)	0.22 (0.20)	0.41 (0.39)

c) Statistical robustness - Mean correlation coefficient (MCC) computed on the test set

	z_{TP}	z_{IO}	z_{PR1}	z_{PR2}
DAG-VAE	0.97 ± 0.03	0.90 ± 0.05	0.93 ± 0.08	0.90 ± 0.06

second dimension, z_{PR2} , captures a slightly asymmetric East-West dipole response.

Next, we evaluate the performance of the DAG-VAE in comparison to the three baselines introduced in Section 3: Principal component analysis combined with regression (PCA), indices with a regression on regional average precipitation (Indices v1), and indices with grid-point-wise regression (Indices v2). Results are shown in Table 1. We first assess how well the reduced representations capture variability in the original input space, quantified using the root mean squared error (RMSE) of the reconstructed data with respect to the original input data (Table 1a). Since the indices cannot reconstruct the original space as such, the DAG-VAE is only compared to PCA here. Here, the DAG-VAE outperforms PCA, i.e. the reconstruction loss is lower. This result is in line with the visualisation of the latent dimensions shown in Figure 3, which showed that the nonlinear dimensionality reduction largely captures the main modes of variability but is able to better represent the spatial asymmetries. Both methods show a large variance in the reconstruction loss, quantified by the standard deviation shown in Table 1. This is due to the imposed constraint of one/two dimensional representation, which will not be able to reconstruct patterns of SST anomalies not directly linked to the main mode of variability.

We furthermore assess the ability of the reduced dimensions of the tropical Pacific and Indian Ocean to predict precipitation over the GHA, evaluated using the Anomaly Correlation Coefficient, as well as the R^2 of total precipitation over the region. R^2 is defined as the ratio of the residual sum of squares to the total sum of squares subtracted from 1. With anomaly correlations around $r = 0.68$, DAG-VAE outperforms both PCA ($r = 0.51$) and indices with regionally averaged precipitation ($r = 0.39$) or grid-point-wise regression ($r=0.50$) in terms of the ability of the reduced representations to predict precipitation, on both the full and test data. This improved performance can be attributed to the joint learning of reduced representations and causal inference, highlighting the potential of both the approach in general and this method specifically to find predictable components of seasonal teleconnections.

The statistical robustness of the DAG-VAE representations is assessed through the mean correlation coefficient of the latent dimensions identified when training the neural network multiple times [Brouillard et al., 2024] which is high, indicating that the mean of the latent dimensions is statistically robust and that the identifiability argued based on Shen et al. [2022] and Lachapelle et al. [2022] holds empirically.

Overall, the DAG-VAE method identifies reduced representations that are both dynamically interpretable and improve upon existing linear approaches in terms of reconstructing the input space and predicting the target variable, precipitation.

4.2 Estimating causal response patterns in seasonal hindcasts

Based on the evaluation conducted in the previous section, we now use the DAG-VAE model trained on seasonal hindcasts to disentangle the direct causal effects of variability in each of the two ocean basins on the GHA short rains. To this end, we simulate intervention experiments in the latent space of the DAG-VAE, setting one of the ocean basins to climatology and evaluating the effect of variability in the other.

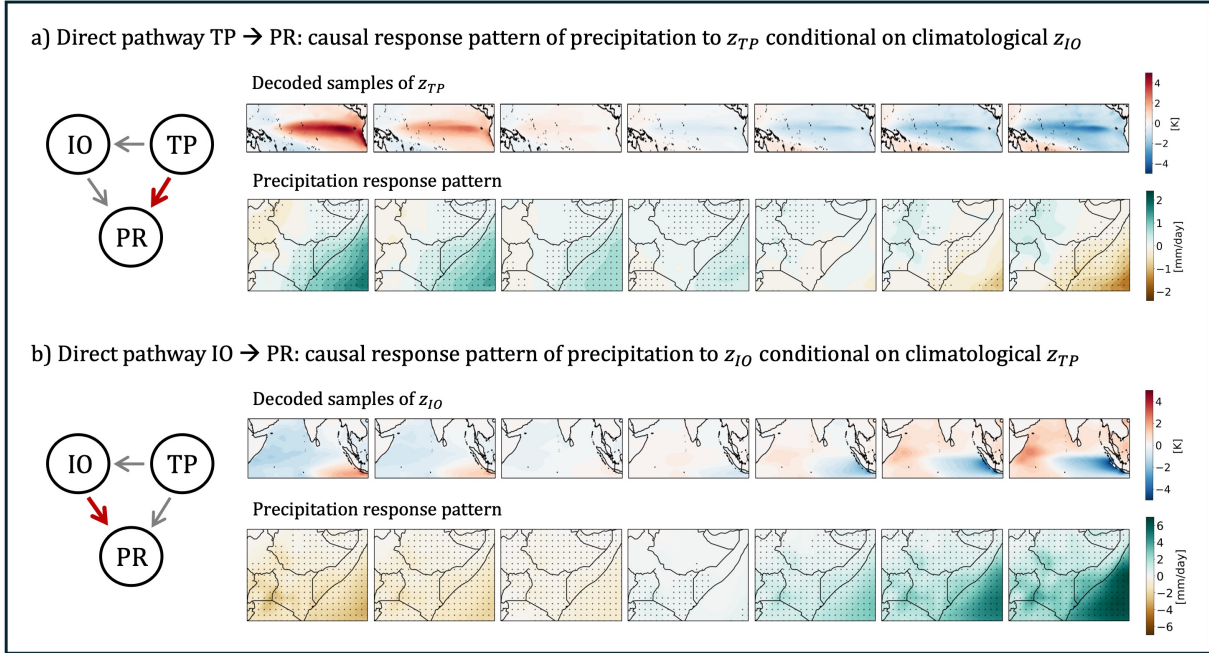


Figure 4: Intervention experiments conducted using DAG-VAE trained on SEAS5. Stippling indicates anomalies whose sign is consistent across 25 training runs, sampling the uncertainty introduced through the initial weights. a) The latent variable representing SSTs in the Indian Ocean, z_{IO} , is set to climatological (neutral) conditions, and samples are drawn from the latent variable representing SSTs in the Pacific, z_{TP} , shown in the top row after decoding. The effect of this intervention on precipitation over the GHA is estimated using the causal model fit in the latent space and shown in the bottom row, aligned to the corresponding sample s of z_{TP} . b) Here, z_{TP} is set to neutral conditions and samples are drawn from z_{IO} (top row), with the corresponding effect on precipitation over the GHA shown in the bottom row.

This approach of setting one ocean basin to climatological conditions resembles the experimental set-up in MacLeod et al. [2021], who study the effect of both realistic and box heating experiments in each of the basins using the ECMWF Integrated Forecasting System (IFS), cycle CY41R1 at T255, against which we benchmark our results. MacLeod et al. [2021] find wet/dry conditions over the entire GHA in response to isolated SST replacement in the Indian Ocean, and a precipitation dipole in response to isolated SST replacement in the Indian Ocean with wet anomalies off the coast and dry anomalies inland in response to El Niño (opposite for La Niña). Given that we are using the same forecasting model, albeit of a slightly later version, we would expect to find similar results to the SST replacement experiments, so long as our assumptions about the physical mechanisms involved are correct.

To estimate the direct effect of the Indian Ocean on precipitation over the GHA, we set the Pacific to climatological conditions defined as the absence of anomalies, and estimate precipitation response patterns based on sampling conditions in the Indian Ocean. These response patterns are estimated using the causal graph fit in the latent space of the model, and represent the spatial causal effect estimated by the DAG-VAE. We proceed equivalently to quantify the direct effect of the Pacific by fixing the Indian Ocean to climatological conditions and estimate precipitation response patterns to variations in the Pacific. Results for both experiments are shown in Figure 4.

We find that the DAG-VAE is able to recover the results of the SST replacement experiments: the direct effect of a positive IOD event is a wet anomaly over the entire region, whereas the effect of a negative IOD event is a region-wide dry anomaly (Fig 4b). The direct effect of ENSO is weaker (note the different colorbar range), and the precipitation response is an east-west dipole with dry anomalies inland and wetting off the coast in response to El Niño, and vice-versa in response to La Niña (Fig. 4a). Further evaluation of the mechanism underlying these two distinct precipitation response patterns conducted by MacLeod et al. [2021] finds that without the additional IOD anomaly, zonal wind anomalies induced by El Niño extend further inland, inhibiting deep convection associated with the pIOD, but inducing off-coast advection-driven positive rainfall anomalies.

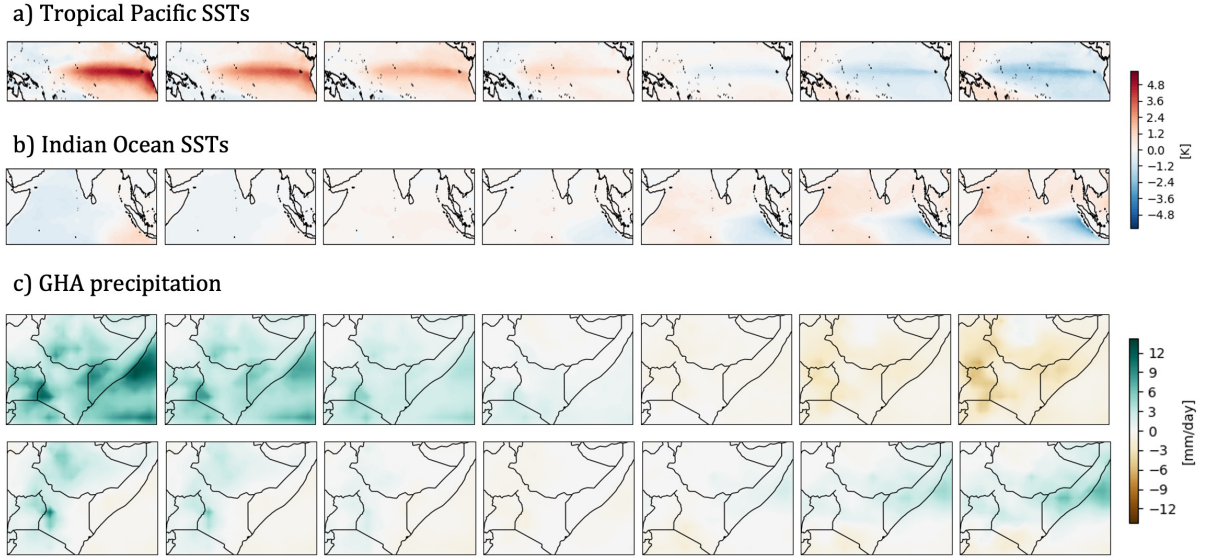


Figure 5: Same as Figure 3, but for ERA5.

Overall, we show that the DAG-VAE method is able to attribute different precipitation response patterns to variability from different ocean basins, recovering results from SST replacement experiments conducted by MacLeod et al. [2021] which represent a widely-used approach to studying the causal effects of teleconnections. The ability of the DAG-VAE trained on seasonal hindcasts to both outperform existing linear methods in terms of reconstruction and prediction, as well as recover results of SST replacement experiments, further shows the benefit of jointly identifying physically interpretable reduced representations and their teleconnections in a data-driven causal framework. Disentangling these two distinct precipitation response patterns, and in particular recovering the dipole response to ENSO, would not have been possible using indices, such as the Niño3.4 index, Dipole Mode Index and regionally averaged precipitation over the GHA used, for example, in Kolstad and MacLeod [2022], as the average of the precipitation dipole response pattern could not have been distinguished from no anomaly. In approaches such as PCA combined with lasso regression or grid-point wise regression, the identified patterns would have been linear, i.e. could not have captured asymmetry in the opposite responses to positive/negative ENSO or IOD events, and would have explained less spatial variability.

4.3 Causal representations and response patterns learned in reanalysis data

So far, we have trained and evaluated the DAG-VAE on the ensemble of seasonal hindcasts. This allowed us to sample a wider range of plausible ENSO and IOD events and their respective response patterns, and compare our results directly to the SST replacement experiments. However, besides being computationally less expensive, a key benefit of the data-driven approach to studying causal response patterns presented here is that it can also be applied to observations or reanalysis data.

We now train the model on ERA5 reanalysis data and compare both the reduced representations and the causal response patterns identified to those found in SEAS5. We implement this training as a fine-tuning of the model weights trained on SEAS5 data as specified in Section 3. This is based on the assumption that although the seasonal hindcasts have known biases in both modes of variability and their teleconnections, the reanalysis-based representations can be found in the neighbourhood of the seasonal model-based representations. As for SEAS5, the model is trained 25 times to investigate uncertainty across initial conditions.

Figure 5 shows the causal representations identified in reanalysis data. While qualitatively consistent, we find slight differences in the representations identified in ERA5 compared to those identified in SEAS5, shown in Figure 3, highlighting known biases in SEAS5. Both ENSO and the IOD exhibit a higher positive skewness in reanalysis data compared to seasonal hindcasts. Furthermore, the positive SST anomalies associated with El Niño, and the negative SST anomalies associated with a positive Indian Ocean Dipole extend less far east. The reduced representations of precipitation show more spatial disaggregation, and, in the case of the first dimension, less strong wet anomalies over the ocean but stronger anomalies over the land. Furthermore, the second latent precipitation dimension no longer shows

Table 2: Same as Table 1, but for ERA5.

1) Reconstruction loss - Root Mean Squared Error (RMSE)

	Tropical Ocean SSTs	Indian Ocean SSTs	GHA precipitation
DAG-VAE	0.25 ± 0.16 (0.23 ± 0.16)	0.47 ± 0.38 (0.45 ± 0.37)	0.29 ± 0.22 (0.31 ± 0.24)
PCA	0.32 ± 0.21	0.62 ± 0.56	0.40 ± 0.30

2) Predictive performance - GHA precipitation

	DAG-VAE	PCA	Indices v1	Indices v2
Anomaly Correlation Coefficient	0.53 (0.27)	0.48 (0.17)	0.44 (0.2)	0.49 (0.21)
R^2 total precipitation	0.58 (0.47)	0.43 (-0.63)	0.48 (-0.26)	0.48 (-0.25)

3) Statistical robustness - Mean correlation coefficient (MCC) across model runs on test set

	z_{TP}	z_{IO}	z_{PR1}	z_{PR2}
DAG-VAE	0.98 ± 0.02	0.87 ± 0.07	0.98 ± 0.01	0.81 ± 0.13

a symmetric East-West dipole as it did for SEAS5.

Table 2 again compares the DAG-VAE to the three baselines: PCA-regression (PCA), index-based regression to regionally averaged precipitation (Indices v1) and grid-cell wise index-based regression (Indices v2). As in SEAS5, the DAG-VAE outperforms both PCA and index regressions in terms of reconstruction loss and predictive performance. In all three baseline methods, the performance of the prediction drops sharply when evaluated over the chosen testing period (1981-1990), attaining negative R^2 values. While the performance of the DAG-VAE method also drops, it retains a higher performance in both the ACC and R^2 , indicating a higher statistical robustness of the method in this application.

Next, we estimate the direct causal response patterns in precipitation to teleconnections from the two ocean basins, using the approach presented in Section 4.2. Results are shown in Figure 6, in the same format as the results for SEAS5 presented in Figure 4. We find that the direct response of precipitation to the IOD is qualitatively similar in ERA5 compared to SEAS5, a region-wide wetting/drying response. However, the wet response is less intense than in SEAS5 over the ocean and the spatial patterns are slightly different and in some cases nonlinear: the regions with the strongest wet response are located further South and over the ocean, compared to the region with the strongest dry response which is located more towards the East and North, over Uganda and South Sudan. The North-East corner of the selected region over South Sudan furthermore does not seem to exhibit a detectable wet response to El Niño, but exhibits a dry response to La Niña.

The direct response to variability in the tropical Pacific, however, differs in ERA5 compared to SEAS5. In SEAS5, the direct response to ENSO is a precipitation dipole, consistent with the results of MacLeod et al. [2021]. In ERA5, on the other hand, we do not recover this dipole. Rather, we find a region-wide dry anomaly in response to La Niña with a similar spatial pattern but weaker amplitude (note different axes) as the response to a negative IOD event. The direct precipitation response to El Niño is a slightly weaker wet anomaly located inland over Kenya, Uganda and North Tanzania. This pattern was not shown to be sensitive to different train-test splits of the data, training over the entire period considered in this paper (1981-2023), or training on reanalysis data extending back to 1940, although the region with a consistent response across model runs (indicated through stippling in Figure 6) shifts slightly (not shown).

Overall, this section shows that the DAG-VAE method introduced here can be applied to reanalysis or observational data and recover consistent representations and response patterns across model runs. Consistent with SEAS5, the method outperforms linear baseline methods in terms of both reconstruction and prediction, and recovers a spatial precipitation response that is statistically more robust when evaluated over a period that the model was not trained on. The difference in the response patterns between SEAS5 and ERA5, discussed further in Section 5, highlights the benefit of data-driven approaches for analysing the causal effects of joint teleconnections and can be used to diagnose and correct biases in seasonal forecasts as well as climate projections.

4.4 Data-driven counterfactuals of seasonal precipitation based on reanalysis data

Having attributed precipitation response patterns over the GHA to variability in the two ocean basins individually, we now use our causal model to generate seasonal counterfactuals. A counterfactual provides the answer to a ‘what would

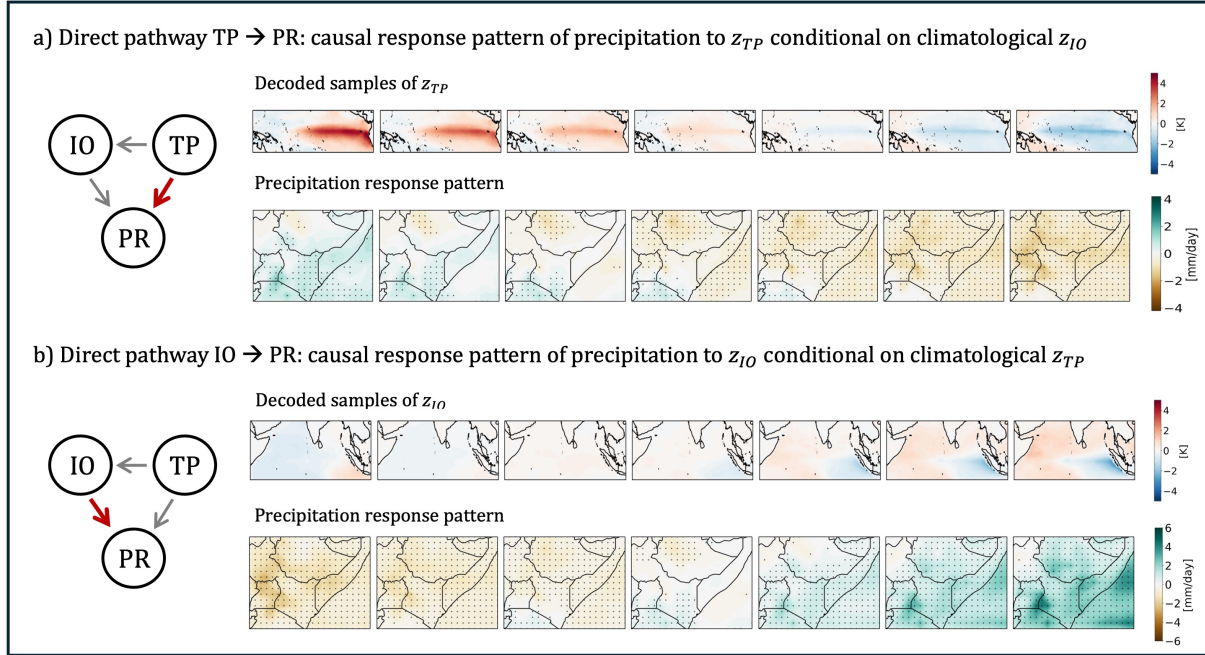


Figure 6: Same as Figure 4 but for ERA5: intervention experiments conducted using DAG-VAE trained on ERA5. Stippling indicates anomalies whose sign is consistent across 25 training runs.

have happened if' question, such as what would have happened if the strong El Niño of 2015 had co-occurred with the strong positive IOD of 2019. Here, we study the counterfactual effects of recent extreme ENSO and IOD events, focusing on the short rains in 2010 (La Niña, negative IOD), 2015 (strong El Niño, moderately positive IOD) and 2019 (neutral ENSO, strong positive IOD). Figure 7 shows the precipitation anomalies resulting from combining the anomalies from the tropical Pacific and Indian Ocean basins from the selected years and estimating their joint effect on precipitation using the causal graph in the latent space of the DAG-VAE trained on ERA5.

Generating counterfactuals requires specifying the noise terms of the model to the event - in this case, the season - in question. In our context, the noise terms are all other processes driving precipitation over the GHA, including subseasonal drivers such as the Madden-Julian Oscillation. Based on the linearity between the predictive relationships in the latent space, counterfactual states in the two ocean basins are assumed to be additive to these other processes. Figure 7 therefore shows the additive counterfactual effect introduced through the interaction of different seasonal drivers. Here, we do not quantify the probability of these different states of the Indian and tropical Pacific Oceans co-occurring.

In the three example seasons investigated here, we find that the dry anomaly associated with the 2010 La Niña would have still been a dry anomaly if it had co-occurred with the moderate positive IOD of 2015, whereas the response would have been spatially disaggregate if it had co-occurred with the strong positive IOD of 2019. If the 2019 IOD, on the other hand, had co-occurred with the strong El Niño event of 2015, the resulting precipitation anomalies would have been even stronger than those actually observed in 2019 which led to flooding and already ranked among the wettest historically observed short rain seasons. In turn, the negative IOD event of 2010 would have caused wide-spread dry anomalies irrespective of the co-occurring ENSO event, albeit of different magnitudes.

In summary, the counterfactual analysis presented here permits the generation of plausible but unseen extreme short rain seasons consistent with large-scale drivers, with possible applications for forecast-based action and scenario planning.

5 Discussion and Conclusion

This paper presents the DAG-VAE method for jointly dimensionality reducing high-dimensional processes in the climate system and disentangling their causal relations. Combining causal inference with deep learning, the method

Seasonal data-driven counterfactuals of the short rains over the GHA

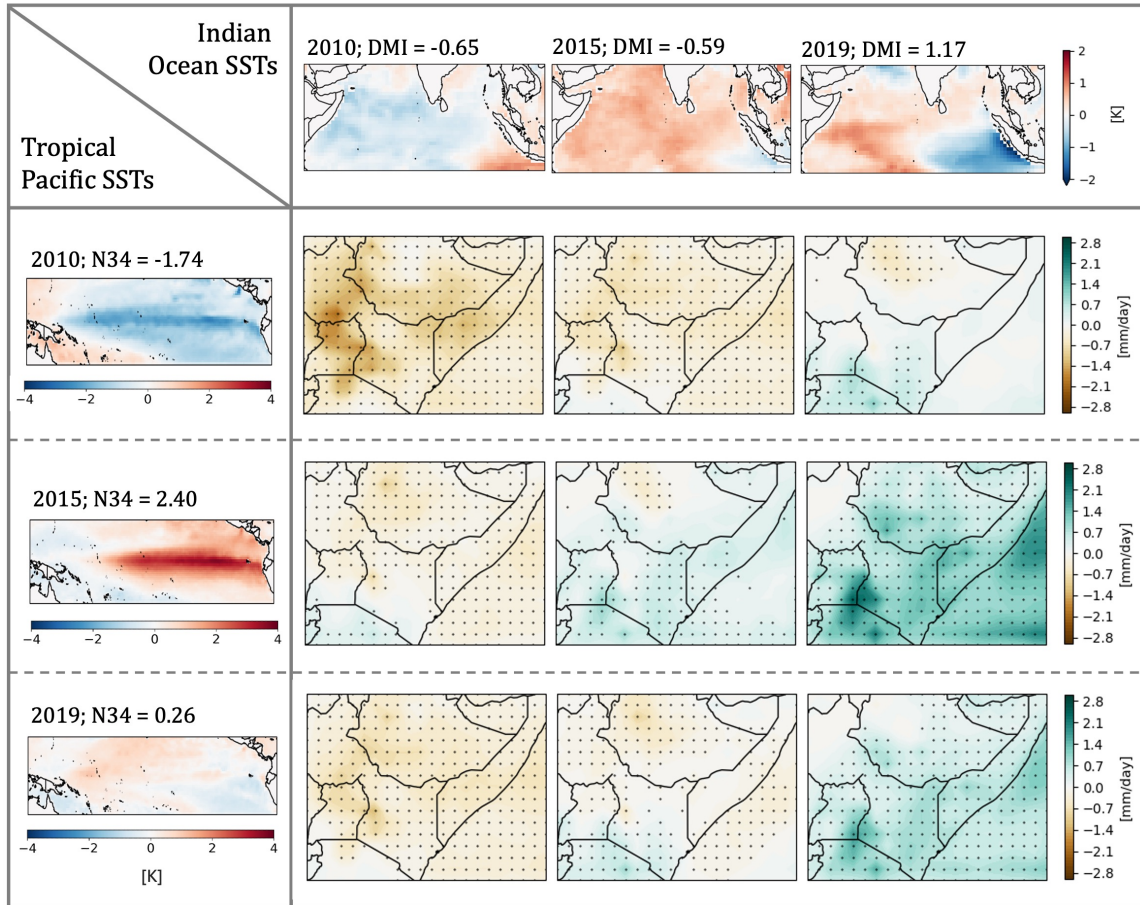


Figure 7: Factual and counterfactual anomalies for three recent short rain seasons in the years 2010, 2025, and 2019 based DAG-VAE trained on ERA5. Precipitation anomalies on the diagonal indicate predicted anomalies given the actually observed conditions. Additive counterfactuals are created by encoding the respective ENSO and IOD anomalies predicted in September into the latent space of the DAG-VAE, and predicting the precipitation response using the causal graph. Stippling indicates anomalies whose sign is consistent across 25 training runs, sampling the uncertainty introduced through the initial weights.

identifies causal relations in a reduced space using variational inference, building on targeted dimensionality reduction approaches developed in Spuler et al. [2024a, 2025] and recent progress in the field of causal representation learning. We apply the method to address the question of whether a direct influence from the tropical Pacific on the short rains over the Greater Horn of Africa (GHA) exists, or whether the teleconnection is mediated entirely by the response of the Indian Ocean.

The architecture is first trained on seasonal hindcasts and subsequently fine-tuned on ERA5 reanalysis. In both cases, the DAG-VAE method outperforms three linear baseline methods in terms of representing variability of the high-dimensional input fields, as well as in the out-of-sample predictive skill of precipitation given its causal parents (Tables 1 and 2). Visualising the respective latent spaces, we find that the DAG-VAE method recovers known modes of variability in the tropical Pacific and Indian Ocean, the El Niño Southern Oscillation (ENSO) and the Indian Ocean Dipole (IOD) (Figures 3 and 5). Due to the nonlinearity of the dimensionality reduction, the DAG-VAE method is able to capture the spatial asymmetry between positive and negative ENSO and IOD patterns in a single latent dimension. We find that compared to ERA5, SEAS5 appears to underestimate the positive skewness of ENSO and the IOD, and overestimate the amplitude of the IOD, consistent with previous findings [Timmermann et al., 2018, Gler et al., 2025].

Next, we attribute the direct causal response pattern of precipitation to teleconnections from the two ocean basins using the reduced-order model identified by the DAG-VAE. In a data-driven model experiment, we constrain one of the ocean basins to climatological conditions and simulate the precipitation response to variability in the other basin. Trained on SEAS5, we find that DAG-VAE is able to recover the results found in SST replacement experiments conducted by MacLeod et al. [2021]: a region-wide wetting/drying response to direct influence from the IOD, and a precipitation dipole response of weaker amplitude in direct response to ENSO (Figure 4). The ability of the proposed approach to identify a response pattern consistent with SST replacement experiments provides evidence for the suitability of the approach, as well as the causal graph hypothesized in this application.

However, evaluating the direct effects from the two ocean basins in ERA5 reanalysis data, we do not find evidence for a dipole response pattern to ENSO. Rather, the direct response to La Niña is a region-wide dry response of weaker amplitude than the direct response to a negative Indian Ocean Dipole, and the response to El Niño emerges as a weak wet response primarily over the South-West of the region. This difference between SEAS5 and ERA5 can be due to model biases in the seasonal hindcasts, as well as sample size issues in ERA5. Considering model biases, MacLeod et al. [2021] discuss a too-strong response of the IOD to variability in the tropical Pacific, as well as mean-state biases in precipitation and the zonal winds over the Indian Ocean, both of which could influence the precipitation signal attributed to the Pacific Ocean [Mayer et al., 2024]. Investigating potential sources of this discrepancy further is beyond the scope of this paper and will be left to future work. Considering sample size issues, the consistency of the identified pattern when training over different time periods provides evidence for the statistical robustness of this result. However, other sensitivities could remain, introduced for example through the choice of dataset. In particular, recent publications find substantial differences across observational and reanalysis products over the Indian Ocean even after 1990 [Wang et al., 2024a, Jain et al., 2025], as well as precipitation biases in ERA5 reanalysis data over the region [Steinkopf and Engelbrecht, 2022].

Finally, we condition on extreme ENSO and IOD states observed in the recent past to simulate counterfactual short rain seasons (Figure 7). We find, for instance, that the short rain season of 2019 which led to wide-spread flooding could have been worse, if an El Niño event of the magnitude and spatial pattern of 2015 had occurred in this year. Overall, the counterfactual analysis presented here exemplifies an approach to generating extreme short rain seasons consistent with large-scale drivers that could be used for scenario planning for unseen events in the humanitarian sector and government.

In terms of the dynamical mechanisms considered, we focus on the average causal effects at seasonal timescales in this paper. However, it is known that these seasonal teleconnections are influenced by variability on other timescales that could be explored in future work: in particular, they are modulated by decadal variability such as the Pacific Decadal Oscillation and anthropogenic climate change, and themselves modulate subseasonal teleconnections such as the Madden-Julian Oscillation which is known to influence precipitation over the GHA [Clark et al., 2003, Kebacho, 2021, Nana et al., 2025a, Wainwright et al., 2021]. The present analysis must therefore be interpreted as estimating causal effects conditional on the timescale (seasonal) and season (October to December) studied. Furthermore, the counterfactual analysis conducted here is conditional on the assumption that the effect of ENSO and the IOD is additive to other drivers of extreme precipitation over the GHA such as the MJO. In addition, the Indian Ocean Dipole is known to peak between September and November, implying that the Indian Ocean Basin Mode, which peaks later in the year, might influence the results we find for October to December [Cai et al., 2019]. We conducted a sensitivity analysis excluding the month of December from our data and found that the results do not change qualitatively (not shown).

The method as it is currently implemented is suitable for studying causal processes at predefined time lags [Kretschmer et al., 2021]. In future work, the method could be extended to study interactions between multiple time-lags that are not hypothesized a priori [Girin et al., 2021, Boussard et al., 2023]. Furthermore, potential synergies with existing linear approaches in climate science that aim to infer governing equations for high-dimensional systems could be explored. For example, linear inverse models and the associated principal oscillation patterns aim to identify deterministic linear dynamics subject to stochastic forcing within the often linearly dimensionality-reduced space of principal components [Kido et al., 2023, Hasselmann, 1988, Kwasniok, 2022, Albers and Newman, 2019]. Furthermore, a range of dynamical systems-based approaches has been used to study reduced representations of teleconnections in the climate system [Ghil and Sciamarella, 2023]. In addition, deep learning methods have, in recent years, led to significant advances in the field of equation discovery [Brunton et al., 2016, Brunton and Kutz, 2024], the application of which in climate science has been discussed by Huntingford et al. [2025].

The latent representations identified by this architecture are inherently interpretable and do not require application of explainable AI (XAI) methods such as Shapley values which are known to show architecture-dependent performance differences [Bommer et al., 2024]. Here, the choice is made deliberately to instead constrain the latent space and jointly optimise its representativeness and prediction skill to discover causal connections in the latent space, rather than optimise predictive performance for which other deep learning approaches would be more suitable.

Overall, we present a data-driven approach to study teleconnections based on observational data that can be used complementary to model experiments. In this paper, we demonstrate the ability of the method to estimate spatial causal response patterns and generate data-driven counterfactuals at seasonal timescales. The findings of this paper could find application in the development of early-warning based action in response to ENSO or IOD forecasts over the Greater Horn of Africa, as well as in the planning for scenarios or storylines of plausible worst-case events [Kelder et al., 2025]. Furthermore, the spatial response patterns identified in reanalysis data could be used to further investigate and correct model biases in seasonal forecasts [Spuler et al., 2024b]. More broadly, the issue of investigating teleconnections between high-dimensional spatiotemporal processes and the pitfalls of dimensionality-reducing processes prior to studying their teleconnections, has been noted in a wide range of publications [Capotondi et al., 2015, Mindlin et al., 2023, Breul et al., 2023], highlighting the potential of the DAG-VAE method to application in other domains of climate dynamics research.

Acknowledgements: This research has been supported by the University of Reading (Advancing the Frontiers of Earth System Prediction (AFESP) Doctoral Training Programme) as well as the European Commission, Horizon Framework Programme (XAIDA (Extreme Events: Artificial Intelligence for Detection and Attribution), grant agreement no. 101003469 and EXPECT (Towards an Integrated Capability to Explain and Predict Regional Climate Changes), grant agreement no. 101137656). The authors thank Jakob Wessel for useful discussions and feedback.

Data availability statement: ERA5 reanalysis data [Hersbach et al., 2020] and SEAS5 seasonal hindcast data [Johnson et al., 2019] were downloaded from the Copernicus Climate Change Service (C3S) (2025). The results contain modified Copernicus Climate Change Service information 2020. Neither the European Commission nor ECMWF is responsible for any use that may be made of the Copernicus information or data it contains. The data underlying the findings is published on Zenodo doi:10.5281/zenodo.17779596.

6 Appendix A: Trend exploration in seasonal hindcasts

Both seasonal and reanalysis data are detrended prior to studying the seasonal teleconnections. We subtract the spatially averaged trend to retain the spatial structure of the trend as it influences the teleconnection studied. Training the model with either non-detrended data or grid-point-wise detrended data does not change the results qualitatively, meaning that the precipitation response patterns shown in Figures 4 and 6 remain similar, and the method still outperforms the baselines investigated (Tables 1 and 2). The grid-point-wise linear trend in SEAS5 is shown in Figure 8.

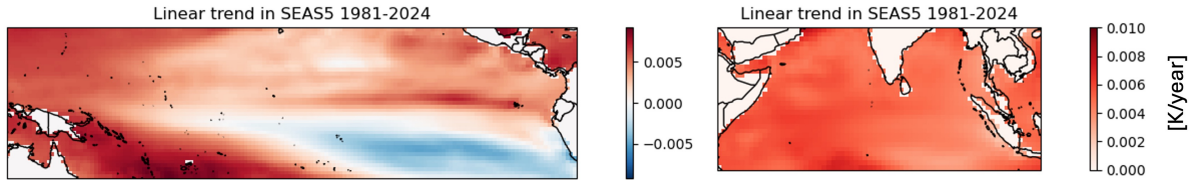


Figure 8: Gridpoint wise trend in SEAS5 averaged across leadtimes.

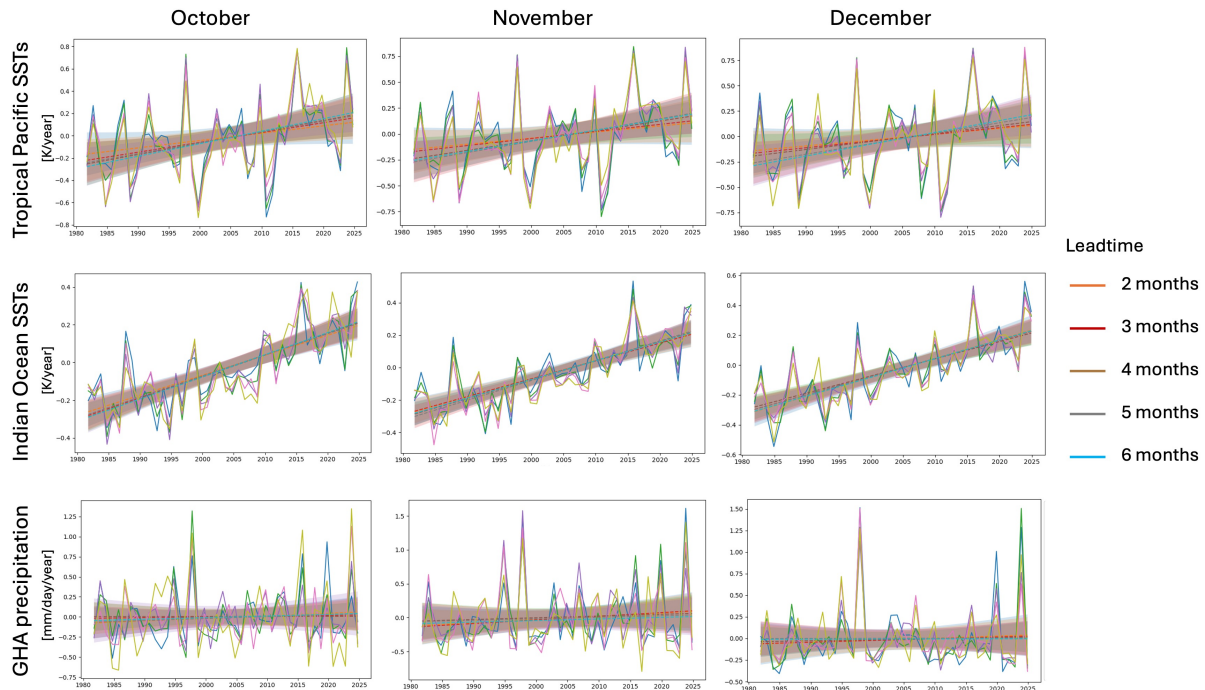


Figure 9: Leadtime dependence of area average trend in SEAS5.

We also investigate the dependence of the area-averaged trend on the leadtime of the seasonal hindcast, based on recent findings that the El Niño-like trend pattern emerges at later leadtimes in seasonal hindcasts [Mayer et al., 2025]. Results are shown in Figure 9. We find that trend of the ensemble mean indeed varies with leadtime over the tropical Pacific (dashed lines). However, bootstrapping this estimate across ensemble members, we find that the uncertainty in the trend estimate is large compared to the difference in the means. We therefore decide to subtract the mean trend across leadtimes, rather than a separate trend for each leadtime.

7 Appendix B: Experiments, loss function and architecture details

A range of implementations of the architecture were developed and tested. We used three separate encoder/decoder structures to identify physically interpretable latent spaces that would enable separate interventions in each of them. In experiments conducted with a single latent space for all three variables, we found that the modes in the Indian and

tropical Pacific Ocean collapsed, and that the reconstruction loss for precipitation compared unfavorably to the model version with separate latent spaces, presumably due to the different properties of its probability distribution.

We also tested architectures with higher-dimensional latent spaces (4-10 dimensions per variable) and found qualitatively similar response patterns, however without being able to guarantee identifiability based on Lachapelle et al. [2022]. Finally, we also developed a version of the architecture that included separate noise dimensions in the latent space of precipitation that are independent of ENSO and IOD. While this version of the architecture also converged well, we here decided to omit these additional dimensions. As they were not required for our studying the research questions asked in this paper, a simpler architecture was seen as preferable.

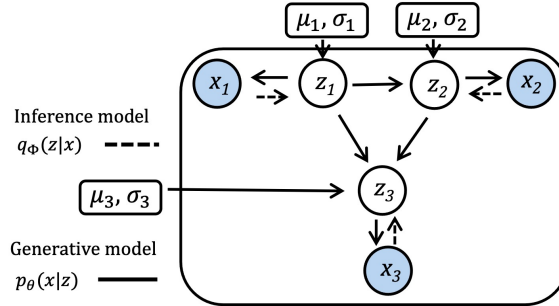


Figure 10: DAG-VAE architecture visualised as a probabilistic graphical model.

To obtain the results presented in this paper, we trained the architecture visualised as a graphical model in Figure 10. Each encoder / decoder pair was implemented using three dense layers of decreasing dimensionality of 256, 128, and 64, respectively. A batch size of 128 and the ReLU activation function are chosen. For the implementation of the neural network architectures, the Python package keras [Chollet, 2015] was used. For a number of the evaluation metrics as well as the implementation of the two linear methods, the Python package scikit-learn [Pedregosa et al., 2011] was employed. The following weights were multiplied to the reconstruction loss terms: $\beta_{TP} = 0.2$, $\beta_{IO} = 0.3$ and $\beta_{PR} = 0.8$ to balance the difference in reconstruction loss resulting from the different area sizes.

For SEAS5, the model is trained 25 times for 100 epochs initialized with random weights with a learning rate of 0.001, and a lasso regularization parameter of 0.01 in the latent space, applying a train-validation-test split of 70%-15%-15% and ensuring that data from one season is only part of one of the three datasets. For ERA5, the model is trained 25 times initialized from the weights of the trained SEAS model with a learning rate of 0.0005 and a lasso regularization parameter of 0.01 in the latent space, applying a train-test split of 80-20%.

References

- John R. Albers and Matthew Newman. A Priori Identification of Skillful Extratropical Subseasonal Forecasts. *Geophysical Research Letters*, 46(21):12527–12536, 2019. ISSN 1944-8007. doi:10.1029/2019GL085270. URL <https://onlinelibrary.wiley.com/doi/abs/10.1029/2019GL085270>. eprint: <https://onlinelibrary.wiley.com/doi/pdf/10.1029/2019GL085270>.
- Joseph J. Barsugli and David S. Battisti. The Basic Effects of Atmosphere–Ocean Thermal Coupling on Midlatitude Variability. February 1998. ISSN 1520-0469. URL https://journals.ametsoc.org/view/journals/atsc/55/4/1520-0469_1998_055_0477_tbeoao_2.0.co_2.xml. Section: Journal of the Atmospheric Sciences.
- Jonathan D. Beverley, Matthew Newman, and Andrew Hoell. Climate model trend errors are evident in seasonal forecasts at short leads. *npj Climate and Atmospheric Science*, 7(1):285, November 2024. ISSN 2397-3722. doi:10.1038/s41612-024-00832-w. URL <https://www.nature.com/articles/s41612-024-00832-w>. Publisher: Nature Publishing Group.
- Emily Black. The relationship between Indian Ocean sea–surface temperature and East African rainfall. *Philosophical Transactions of the Royal Society A: Mathematical, Physical and Engineering Sciences*, January 2005. doi:10.1098/rsta.2004.1474. URL <https://royalsocietypublishing.org/doi/10.1098/rsta.2004.1474>. Publisher: The Royal Society.
- Emily Black, Julia Slingo, and Kenneth R. Sperber. An Observational Study of the Relationship between Excessively Strong Short Rains in Coastal East Africa and Indian Ocean SST. January 2003. ISSN 1520-0493. URL https://journals.ametsoc.org/view/journals/mwre/131/1/1520-0493_2003_131_0074_aosotr_2.0.co_2.xml. Section: Monthly Weather Review.
- Philine Lou Bommer, Marlene Kretschmer, Anna Hedström, Dilyara Bareeva, and Marina M.-C. Höhne. Finding the Right XAI Method—A Guide for the Evaluation and Ranking of Explainable AI Methods in Climate Science. June 2024. doi:10.1175/AIES-D-23-0074.1. URL <https://journals.ametsoc.org/view/journals/aies/3/3/AIES-D-23-0074.1.xml>. Section: Artificial Intelligence for the Earth Systems.
- Julien Boussard, Chandni Nagda, Julia Kaltenborn, Charlotte Emilie Elektra Lange, Philippe Brouillard, Yaniv Gurwicz, Peer Nowack, and David Rolnick. Towards Causal Representations of Climate Model Data, December 2023. URL <http://arxiv.org/abs/2312.02858>. arXiv:2312.02858 [cs].
- Philipp Breul, Paulo Ceppi, and Theodore G. Shepherd. Revisiting the wintertime emergent constraint of the southern hemispheric midlatitude jet response to global warming. *Weather and Climate Dynamics*, 4(1):39–47, January 2023. doi:10.5194/wcd-4-39-2023. URL <https://wcd.copernicus.org/articles/4/39/2023/>. Publisher: Copernicus GmbH.
- Philippe Brouillard, Sébastien Lachapelle, Julia Kaltenborn, Yaniv Gurwicz, Dhanya Sridhar, Alexandre Drouin, Peer Nowack, Jakob Runge, and David Rolnick. Causal Representation Learning in Temporal Data via Single-Parent Decoding, October 2024. URL <http://arxiv.org/abs/2410.07013>. arXiv:2410.07013 [cs].
- Steven L. Brunton and J. Nathan Kutz. Promising directions of machine learning for partial differential equations. *Nature Computational Science*, 4(7):483–494, July 2024. ISSN 2662-8457. doi:10.1038/s43588-024-00643-2. URL <https://www.nature.com/articles/s43588-024-00643-2>. Publisher: Nature Publishing Group.
- Steven L. Brunton, Joshua L. Proctor, and J. Nathan Kutz. Discovering governing equations from data by sparse identification of nonlinear dynamical systems. *Proceedings of the National Academy of Sciences*, 113(15):3932–3937, April 2016. doi:10.1073/pnas.1517384113. URL <https://www.pnas.org/doi/abs/10.1073/pnas.1517384113>. Publisher: Proceedings of the National Academy of Sciences.
- Wenju Cai, Lixin Wu, Matthieu Lengaigne, Tim Li, Shayne McGregor, Jong-Seong Kug, Jin-Yi Yu, Malte F. Stuecker, Agus Santoso, Xichen Li, Yoo-Geun Ham, Yoshimitsu Chikamoto, Benjamin Ng, Michael J. McPhaden, Yan Du, Dietmar Dommenget, Fan Jia, Jules B. Kajtar, Noel Keenlyside, Xiaopei Lin, Jing-Jia Luo, Marta Martín-Rey, Yohan Ruprich-Robert, Guojian Wang, Shang-Ping Xie, Yun Yang, Sarah M. Kang, Jun-Young Choi, Bolan Gan, Geon-Il Kim, Chang-Eun Kim, Sunyoung Kim, Jeong-Hwan Kim, and Ping Chang. Pantropical climate interactions. *Science*, 363(6430):eaav4236, March 2019. doi:10.1126/science.aav4236. URL <https://www.science.org/doi/10.1126/science.aav4236>. Publisher: American Association for the Advancement of Science.
- Antonietta Capotondi, Andrew T. Wittenberg, Matthew Newman, Emanuele Di Lorenzo, Jin-Yi Yu, Pascale Braconnot, Julia Cole, Boris Dewitte, Benjamin Giese, Eric Guilyardi, Fei-Fei Jin, Kristopher Karnauskas, Benjamin Kirtman, Tong Lee, Niklas Schneider, Yan Xue, and Sang-Wook Yeh. Understanding ENSO Diversity. June 2015. doi:10.1175/BAMS-D-13-00117.1. URL <https://journals.ametsoc.org/view/journals/bams/96/6/bams-d-13-00117.1.xml>. Section: Bulletin of the American Meteorological Society.
- Francois Chollet. Keras. 2015. URL <https://keras.io>.

- Christina Oelfke Clark, Peter J. Webster, and Julia E. Cole. Interdecadal Variability of the Relationship between the Indian Ocean Zonal Mode and East African Coastal Rainfall Anomalies. February 2003. ISSN 1520-0442. URL https://journals.ametsoc.org/view/journals/clim/16/3/1520-0442_2003_016_0548_ivotrb_2.0.co_2.xml. Section: Journal of Climate.
- Giorgia Di Capua, Jakob Runge, Reik V. Donner, Bart van den Hurk, Andrew G. Turner, Ramesh Vellore, Raghavan Krishnan, and Dim Coumou. Dominant patterns of interaction between the tropics and mid-latitudes in boreal summer: causal relationships and the role of timescales. *Weather and Climate Dynamics*, 1(2):519–539, October 2020. doi:10.5194/wcd-1-519-2020. URL <https://wcd.copernicus.org/articles/1/519/2020/>. Publisher: Copernicus GmbH.
- Dietmar Dommenges and Mojib Latif. A Cautionary Note on the Interpretation of EOFs. January 2002. ISSN 1520-0442. URL https://journals.ametsoc.org/view/journals/clim/15/2/1520-0442_2002_015_0216_acnoti_2.0.co_2.xml. Section: Journal of Climate.
- Yan Du, Wenju Cai, and Yanling Wu. A New Type of the Indian Ocean Dipole since the Mid-1970s. February 2013. doi:10.1175/JCLI-D-12-00047.1. URL <https://journals.ametsoc.org/view/journals/clim/26/3/jcli-d-12-00047.1.xml>. Section: Journal of Climate.
- Xianghui Fang, Henk Dijkstra, Claudia Wieners, and Francesco Guardamagna. A Nonlinear Full-Field Conceptual Model for ENSO Diversity. June 2024. doi:10.1175/JCLI-D-23-0382.1. URL <https://journals.ametsoc.org/view/journals/clim/37/14/JCLI-D-23-0382.1.xml>. Section: Journal of Climate.
- Albert S. Fischer, Pascal Terray, Eric Guilyardi, Silvio Gualdi, and Pascale Delecluse. Two Independent Triggers for the Indian Ocean Dipole/Zonal Mode in a Coupled GCM. September 2005. doi:10.1175/JCLI3478.1. URL <https://journals.ametsoc.org/view/journals/clim/18/17/jcli3478.1.xml>. Section: Journal of Climate.
- Michael Ghil and Denisse Sciamarella. Review article: Dynamical systems, algebraic topology and the climate sciences. *Nonlinear Processes in Geophysics*, 30(4):399–434, October 2023. ISSN 1023-5809. doi:10.5194/npg-30-399-2023. URL <https://npg.copernicus.org/articles/30/399/2023/>. Publisher: Copernicus GmbH.
- Laurent Girin, Simon Leglaive, Xiaoyu Bie, Julien Diard, Thomas Hueber, and Xavier Alameda-Pineda. Dynamical Variational Autoencoders: A Comprehensive Review. *Foundations and Trends® in Machine Learning*, 15(1-2):1–175, 2021. ISSN 1935-8237, 1935-8245. doi:10.1561/22000000089. URL <http://arxiv.org/abs/2008.12595>. arXiv:2008.12595 [cs, stat].
- Marimel Gler, Andrew Turner, Linda Hirons, Caroline Wainwright, and Charline Marzin. Systematic biases over the equatorial Indian Ocean and their influence on seasonal forecasts of the IOD. *Climate Dynamics*, July 2025. ISSN 1432-0894. URL <https://centaur.reading.ac.uk/123547/>. Publisher: Springer.
- Lisa Goddard and Nicholas E. Graham. Importance of the Indian Ocean for simulating rainfall anomalies over eastern and southern Africa. *Journal of Geophysical Research: Atmospheres*, 104(D16):19099–19116, 1999. ISSN 2156-2202. doi:10.1029/1999JD900326. URL <https://onlinelibrary.wiley.com/doi/abs/10.1029/1999JD900326>. _eprint: <https://agupubs.onlinelibrary.wiley.com/doi/pdf/10.1029/1999JD900326>.
- Masilin Gudoshava, Caroline Wainwright, Linda Hirons, Hussien S. Endris, Zewdu T. Segele, Steve Woolnough, Zachary Atheru, and Guleid Artan. Atmospheric and oceanic conditions associated with early and late onset for Eastern Africa short rains. *International Journal of Climatology*, 42(12):6562–6578, 2022. ISSN 1097-0088. doi:10.1002/joc.7627. URL <https://onlinelibrary.wiley.com/doi/abs/10.1002/joc.7627>. _eprint: <https://rmets.onlinelibrary.wiley.com/doi/pdf/10.1002/joc.7627>.
- Masilin Gudoshava, George Otieno, Eunice Koech, Herbert Misiani, Jemimah Gacheru Ongoma, Claudio Heinrich-Mertsching, Calistus Wachana, Hussien Seid Endris, Anthony Mwanthi, Mary Kilavi, Emmah Mwangi, Andrew Colman, Douglas Parker, Joseph Nzau Mutemi, Paula Machio, Paulino Omoj Omay, Paul Ombai, Doreen Anande, Alfred Kondowe, Isaac Mugume, Prosper Ayabagabo, Houada Youssouf Houssein, Mahado Salah Waiss, Bekele Abeshu, Ezechiel Kayoya, Mohamud Nor Sharawe, Titike Bahaga, Martin Todd, Zewdu Segele, Zachary Atheru, and Guleid Artan. Advances, gaps and way forward in provision of climate services over the Greater Horn of Africa. *Frontiers in Climate*, 6, January 2024. ISSN 2624-9553. doi:10.3389/fclim.2024.1307535. URL <https://www.frontiersin.org/journals/climate/articles/10.3389/fclim.2024.1307535/full>. Publisher: Frontiers.
- Robin Guillaume-Castel, Paulo Ceppi, Joshua Dorrington, and Benoit Meyssignac. ENSO diversity explains interannual variability of the pattern effect. URL <https://www.authorea.com/users/773945/articles/1296821-enso-diversity-explains-interannual-variability-of-the-pattern-effect?commit=8703cd735992f995e482215adccf6f4ccf72d6f8>.

- Feiyan Guo, Qinyu Liu, S. Sun, and Jianling Yang. Three Types of Indian Ocean Dipoles. April 2015. doi:10.1175/JCLI-D-14-00507.1. URL <https://journals.ametsoc.org/view/journals/clim/28/8/jcli-d-14-00507.1.xml>. Section: Journal of Climate.
- K. Hasselmann. PIPs and POPs: The reduction of complex dynamical systems using principal interaction and oscillation patterns. *Journal of Geophysical Research: Atmospheres*, 93(D9):11015–11021, 1988. ISSN 2156-2202. doi:10.1029/JD093iD09p11015. URL <https://onlinelibrary.wiley.com/doi/abs/10.1029/JD093iD09p11015>. _eprint: <https://onlinelibrary.wiley.com/doi/pdf/10.1029/JD093iD09p11015>.
- Hans Hersbach, Bill Bell, Paul Berrisford, Shoji Hirahara, András Horányi, Joaquín Muñoz-Sabater, Julien Nicolas, Carole Peubey, Raluca Radu, Dinand Schepers, Adrian Simmons, Cornel Soci, Saleh Abdalla, Xavier Abellan, Gianpaolo Balsamo, Peter Bechtold, Gionata Biavati, Jean Bidlot, Massimo Bonavita, Giovanna De Chiara, Per Dahlgren, Dick Dee, Michail Diamantakis, Rossana Dragani, Johannes Flemming, Richard Forbes, Manuel Fuentes, Alan Geer, Leo Haimberger, Sean Healy, Robin J. Hogan, Elías Hólm, Marta Janisková, Sarah Keeley, Patrick Laloyaux, Philippe Lopez, Cristina Lupu, Gabor Radnoti, Patricia de Rosnay, Iryna Rozum, Freja Vamborg, Sebastien Villaume, and Jean-Noël Thépaut. The ERA5 global reanalysis. *Quarterly Journal of the Royal Meteorological Society*, 146(730):1999–2049, 2020. ISSN 1477-870X. doi:10.1002/qj.3803. URL <https://onlinelibrary.wiley.com/doi/abs/10.1002/qj.3803>. _eprint: <https://onlinelibrary.wiley.com/doi/pdf/10.1002/qj.3803>.
- Sebastian Hickman, Ilija Trajkovic, Julia Kaltenborn, Francis Pelletier, Alex Archibald, Yaniv Gurwicz, Peer Nowack, David Rolnick, and Julien Boussard. Causal Climate Emulation with Bayesian Filtering, October 2025. URL <http://arxiv.org/abs/2506.09891>. arXiv:2506.09891 [cs].
- Linda Hirons and Andrew Turner. The Impact of Indian Ocean Mean-State Biases in Climate Models on the Representation of the East African Short Rains. August 2018. doi:10.1175/JCLI-D-17-0804.1. URL <https://journals.ametsoc.org/view/journals/clim/31/16/jcli-d-17-0804.1.xml>. Section: Journal of Climate.
- Chris Huntingford, Andrew J. Nicoll, Cornelia Klein, and Jawairia A. Ahmad. Potential for equation discovery with AI in the climate sciences. *Earth System Dynamics*, 16(2):475–495, March 2025. ISSN 2190-4979. doi:10.5194/esd-16-475-2025. URL <https://esd.copernicus.org/articles/16/475/2025/>. Publisher: Copernicus GmbH.
- Shipra Jain, Thea Turkington, Wee Leng Tan, Chen Schwartz, Adam A. Scaife, and Theodore G. Shepherd. Towards developing an operational Indian ocean dipole warning system for Southeast Asia. *Scientific Reports*, 15(1):14728, April 2025. ISSN 2045-2322. doi:10.1038/s41598-025-99261-9. URL <https://www.nature.com/articles/s41598-025-99261-9>. Publisher: Nature Publishing Group.
- Richard A. Johnson and Dean W. Wichern. *Applied Multivariate Statistical Analysis: Pearson New International Edition*. Pearson Higher Ed, August 2013. ISBN 978-1-292-03757-8. Google-Books-ID: xCipBwAAQBAJ.
- Stephanie J. Johnson, Timothy N. Stockdale, Laura Ferranti, Magdalena A. Balmaseda, Franco Molteni, Linus Magnusson, Steffen Tietsche, Damien Decremé, Antje Weisheimer, Gianpaolo Balsamo, Sarah P. E. Keeley, Kristian Mogensen, Hao Zuo, and Beatriz M. Monge-Sanz. SEAS5: the new ECMWF seasonal forecast system. *Geoscientific Model Development*, 12(3):1087–1117, March 2019. ISSN 1991-959X. doi:10.5194/gmd-12-1087-2019. URL <https://gmd.copernicus.org/articles/12/1087/2019/>. Publisher: Copernicus GmbH.
- Ian T. Jolliffe and Jorge Cadima. Principal component analysis: a review and recent developments. *Philosophical transactions. Series A, Mathematical, physical, and engineering sciences*, 374(2065):20150202, April 2016. ISSN 1364-503X. doi:10.1098/rsta.2015.0202. URL <https://www.ncbi.nlm.nih.gov/pmc/articles/PMC4792409/>.
- Laban Lameck Kebacho. Large-scale circulations associated with recent interannual variability of the short rains over East Africa. *Meteorology and Atmospheric Physics*, 134(1):10, November 2021. ISSN 1436-5065. doi:10.1007/s00703-021-00846-6. URL <https://doi.org/10.1007/s00703-021-00846-6>.
- Timo Kelder, Dorothy Heinrich, Lisette Klok, Vikki Thompson, Henrique M. D. Goulart, Ed Hawkins, Louise J. Slater, Laura Suarez-Gutierrez, Robert L. Wilby, Erin Coughlan de Perez, Elisabeth M. Stephens, Stephen Burt, Bart van den Hurk, Hylke de Vries, Karin van der Wiel, E. Lisa F. Schipper, Antonio Carmona Baéz, Ellen van Bueren, and Erich M. Fischer. How to stop being surprised by unprecedented weather. *Nature Communications*, 16(1):2382, March 2025. ISSN 2041-1723. doi:10.1038/s41467-025-57450-0. URL <https://www.nature.com/articles/s41467-025-57450-0>. Publisher: Nature Publishing Group.
- Ilyes Khemakhem, Diederik P. Kingma, Ricardo Pio Monti, and Aapo Hyvärinen. Variational Autoencoders and Nonlinear ICA: A Unifying Framework, December 2020. URL <http://arxiv.org/abs/1907.04809>. arXiv:1907.04809 [cs, stat].
- Shoichiro Kido, Ingo Richter, Tomoki Tozuka, and Ping Chang. Understanding the interplay between ENSO and related tropical SST variability using linear inverse models. *Climate Dynamics*, 61(3):1029–1048, August 2023. ISSN 1432-0894. doi:10.1007/s00382-022-06484-x. URL <https://doi.org/10.1007/s00382-022-06484-x>.

- Diederik P. Kingma and Max Welling. Auto-Encoding Variational Bayes, 2013. URL <http://arxiv.org/abs/1312.6114>. arXiv:1312.6114 [cs, stat].
- E. W. Kolstad, D. MacLeod, and T. D. Demissie. Drivers of Subseasonal Forecast Errors of the East African Short Rains. *Geophysical Research Letters*, 48(14):e2021GL093292, 2021. ISSN 1944-8007. doi:10.1029/2021GL093292. URL <https://onlinelibrary.wiley.com/doi/abs/10.1029/2021GL093292>. _eprint: <https://onlinelibrary.wiley.com/doi/pdf/10.1029/2021GL093292>.
- Erik W. Kolstad and David MacLeod. Lagged oceanic effects on the East African short rains. *Climate Dynamics*, 59(3):1043–1056, August 2022. ISSN 1432-0894. doi:10.1007/s00382-022-06176-6. URL <https://doi.org/10.1007/s00382-022-06176-6>.
- Erik W. Kolstad, Douglas J. Parker, David A. MacLeod, Caroline M. Wainwright, and Linda C. Hiron. Beyond the regional average: Drivers of geographical rainfall variability during East Africa’s short rains. *Quarterly Journal of the Royal Meteorological Society*, 150(764):4550–4566, 2024. ISSN 1477-870X. doi:10.1002/qj.4829. URL <https://onlinelibrary.wiley.com/doi/abs/10.1002/qj.4829>. _eprint: <https://rmets.onlinelibrary.wiley.com/doi/pdf/10.1002/qj.4829>.
- Marlene Kretschmer, Dim Coumou, Jonathan F. Donges, and Jakob Runge. Using Causal Effect Networks to Analyze Different Arctic Drivers of Midlatitude Winter Circulation. *Journal of Climate*, 29(11):4069–4081, June 2016. ISSN 0894-8755, 1520-0442. doi:10.1175/JCLI-D-15-0654.1. URL <https://journals.ametsoc.org/view/journals/clim/29/11/jcli-d-15-0654.1.xml>. Publisher: American Meteorological Society Section: Journal of Climate.
- Marlene Kretschmer, Giuseppe Zappa, and Theodore G. Shepherd. The role of Barents–Kara sea ice loss in projected polar vortex changes. *Weather and Climate Dynamics*, 1(2):715–730, November 2020. ISSN 2698-4016. doi:10.5194/wcd-1-715-2020. URL <https://wcd.copernicus.org/articles/1/715/2020/>.
- Marlene Kretschmer, Samantha V. Adams, Alberto Arribas, Rachel Prudden, Niall Robinson, Elena Saggioro, and Theodore G. Shepherd. Quantifying Causal Pathways of Teleconnections. *Bulletin of the American Meteorological Society*, 102(12):E2247–E2263, December 2021. ISSN 0003-0007, 1520-0477. doi:10.1175/BAMS-D-20-0117.1. URL <https://journals.ametsoc.org/view/journals/bams/102/12/BAMS-D-20-0117.1.xml>.
- Frank Kwasniok. Linear Inverse Modeling of Large-Scale Atmospheric Flow Using Optimal Mode Decomposition. *Journal of the Atmospheric Sciences*, 79(9):2181–2204, September 2022. ISSN 0022-4928, 1520-0469. doi:10.1175/JAS-D-21-0193.1. URL <https://journals.ametsoc.org/view/journals/atsc/79/9/JAS-D-21-0193.1.xml>. Publisher: American Meteorological Society Section: Journal of the Atmospheric Sciences.
- Sébastien Lachapelle, Pau Rodríguez López, Yash Sharma, Katie Everett, Rémi Le Priol, Alexandre Lacoste, and Simon Lacoste-Julien. Disentanglement via Mechanism Sparsity Regularization: A New Principle for Nonlinear ICA, February 2022. URL <http://arxiv.org/abs/2107.10098>. arXiv:2107.10098 [stat].
- M. Latif, D. Dommenges, M. Dima, and A. Grötzner. The Role of Indian Ocean Sea Surface Temperature in Forcing East African Rainfall Anomalies during December–January 1997/98. December 1999. ISSN 1520-0442. URL https://journals.ametsoc.org/view/journals/clim/12/12/1520-0442_1999_012_3497_troios_2.0.co_2.xml. Section: Journal of Climate.
- Aurélien Liné, Christophe Cassou, Rym Msadek, and Sylvie Pary. Modulation of Northern Europe near-term anthropogenic warming and wetting assessed through internal variability storylines. *npj Climate and Atmospheric Science*, 7(1):1–14, November 2024. ISSN 2397-3722. doi:10.1038/s41612-024-00759-2. URL <https://www.nature.com/articles/s41612-024-00759-2>. Publisher: Nature Publishing Group.
- Lin Liu, Guang Yang, Xia Zhao, Lin Feng, Guoqing Han, Yue Wu, and Weidong Yu. Why Was the Indian Ocean Dipole Weak in the Context of the Extreme El Niño in 2015? June 2017. doi:10.1175/JCLI-D-16-0281.1. URL <https://journals.ametsoc.org/view/journals/clim/30/12/jcli-d-16-0281.1.xml>. Section: Journal of Climate.
- Francesco Locatello, Stefan Bauer, Mario Lucic, Gunnar Rätsch, Sylvain Gelly, Bernhard Schölkopf, and Olivier Bachem. Challenging Common Assumptions in the Unsupervised Learning of Disentangled Representations, June 2019. URL <http://arxiv.org/abs/1811.12359>. arXiv:1811.12359.
- David MacLeod and Cyril Caminade. The Moderate Impact of the 2015 El Niño over East Africa and Its Representation in Seasonal Reforecasts. November 2019. doi:10.1175/JCLI-D-19-0201.1. URL <https://journals.ametsoc.org/view/journals/clim/32/22/jcli-d-19-0201.1.xml>. Section: Journal of Climate.
- David MacLeod, Richard Graham, Chris O’Reilly, George Otieno, and Martin Todd. Causal pathways linking different flavours of ENSO with the Greater Horn of Africa short rains. *Atmospheric Science Letters*, 22(2):e1015, 2021. ISSN 1530-261X. doi:10.1002/asl.1015. URL <https://onlinelibrary.wiley.com/doi/abs/10.1002/asl.1015>. _eprint: <https://onlinelibrary.wiley.com/doi/pdf/10.1002/asl.1015>.

- Annarita Mariotti, Cory Baggett, Elizabeth A. Barnes, Emily Becker, Amy Butler, Dan C. Collins, Paul A. Dirmeyer, Laura Ferranti, Nathaniel C. Johnson, Jeanine Jones, Ben P. Kirtman, Andrea L. Lang, Andrea Molod, Matthew Newman, Andrew W. Robertson, Siegfried Schubert, Duane E. Waliser, and John Albers. Windows of Opportunity for Skillful Forecasts Subseasonal to Seasonal and Beyond. *Bulletin of the American Meteorological Society*, 101(5): E608–E625, May 2020. ISSN 0003-0007, 1520-0477. doi:10.1175/BAMS-D-18-0326.1. URL <https://journals.ametsoc.org/view/journals/bams/101/5/bams-d-18-0326.1.xml>. Publisher: American Meteorological Society Section: Bulletin of the American Meteorological Society.
- Michael Mayer, Magdalena Alonso Balmaseda, Stephanie Johnson, and Frederic Vitart. Assessment of seasonal forecasting errors of the ECMWF system in the eastern Indian Ocean. *Climate Dynamics*, 62(2):1391–1406, February 2024. ISSN 1432-0894. doi:10.1007/s00382-023-06985-3. URL <https://doi.org/10.1007/s00382-023-06985-3>.
- Michael Mayer, Magdalena A. Balmaseda, Frederic Vitart, and Steffen Tietsche. Tropical Pacific Trends in the ECMWF Seasonal System and Implications for Predictions of the 2020–22 Triple-Dip La Niña. *Journal of Climate*, 38(13): 2989–3003, June 2025. ISSN 0894-8755, 1520-0442. doi:10.1175/JCLI-D-24-0467.1. URL <https://journals.ametsoc.org/view/journals/clim/38/13/JCLI-D-24-0467.1.xml>. Publisher: American Meteorological Society Section: Journal of Climate.
- Julia Mindlin, Carolina S. Vera, Theodore G. Shepherd, and Marisol Osman. Plausible Drying and Wetting Scenarios for Summer in Southeastern South America. *Journal of Climate*, -1(aop), August 2023. ISSN 0894-8755, 1520-0442. doi:10.1175/JCLI-D-23-0134.1. URL <https://journals.ametsoc.org/view/journals/clim/aop/JCLI-D-23-0134.1/JCLI-D-23-0134.1.xml>. Publisher: American Meteorological Society Section: Journal of Climate.
- Julia Mindlin, Theodore G. Shepherd, Marisol Osman, Carolina S. Vera, and Marlene Kretschmer. Explaining and predicting the Southern Hemisphere eddy-driven jet. *Proceedings of the National Academy of Sciences*, 122(29): e2500697122, July 2025. doi:10.1073/pnas.2500697122. URL <https://www.pnas.org/doi/10.1073/pnas.2500697122>. Publisher: Proceedings of the National Academy of Sciences.
- Hermann N. Nana, Masilin Gudoshava, Roméo S. Tanessong, Alain T. Tamoffo, and Derbetini A. Vondou. Diverse Causes of Extreme Rainfall in November 2023 over Equatorial Africa, February 2025a. URL <https://egusphere.copernicus.org/preprints/2025/egusphere-2025-76/>.
- Hermann N. Nana, Roméo S. Tanessong, Masilin Gudoshava, and Derbetini A. Vondou. Assessing the ability of the ECMWF seasonal prediction model to forecast extreme September-to-November rainfall events over Equatorial Africa, August 2025b. URL <https://egusphere.copernicus.org/preprints/2025/egusphere-2025-2656/>.
- Sharon E. Nicholson. Climate and climatic variability of rainfall over eastern Africa. *Reviews of Geophysics*, 55(3): 590–635, 2017. ISSN 1944-9208. doi:10.1002/2016RG000544. URL <https://onlinelibrary.wiley.com/doi/abs/10.1002/2016RG000544>. eprint: <https://onlinelibrary.wiley.com/doi/pdf/10.1002/2016RG000544>.
- Christopher H. O’Reilly, Matthew Patterson, Jon Robson, Paul Arthur Monerie, Daniel Hodson, and Yohan Ruprich-Robert. Challenges with interpreting the impact of Atlantic Multidecadal Variability using SST-restoring experiments. *npj Climate and Atmospheric Science*, 6(1):1–12, February 2023. ISSN 2397-3722. doi:10.1038/s41612-023-00335-0. URL <https://www.nature.com/articles/s41612-023-00335-0>. Publisher: Nature Publishing Group.
- Paul I. Palmer, Caroline M. Wainwright, Bo Dong, Ross I. Maidment, Kevin G. Wheeler, Nicola Gedney, Jonathan E. Hickman, Nima Madani, Sonja S. Folwell, Gamal Abdo, Richard P. Allan, Emily C. L. Black, Liang Feng, Masilin Gudoshava, Keith Haines, Chris Huntingford, Mary Kilavi, Mark F. Lunt, Ahmed Shaaban, and Andrew G. Turner. Drivers and impacts of Eastern African rainfall variability. *Nature Reviews Earth & Environment*, 4(4):254–270, April 2023. ISSN 2662-138X. doi:10.1038/s43017-023-00397-x. URL <https://www.nature.com/articles/s43017-023-00397-x>. Number: 4 Publisher: Nature Publishing Group.
- Judea Pearl. Causal inference in statistics: An overview. *Statistics Surveys*, 3(none):96–146, January 2009. ISSN 1935-7516. doi:10.1214/09-SS057. URL <https://projecteuclid.org/journals/statistics-surveys/volume-3/issue-none/Causal-inference-in-statistics-An-overview/10.1214/09-SS057.full>. Publisher: Amer. Statist. Assoc., the Bernoulli Soc., the Inst. Math. Statist., and the Statist. Soc. Canada.
- F. Pedregosa, G. Varoquaux, V. Michel, B. Thirion, O. Grisel, M. Blondel, P. Prettenhofer, R. Weiss, V. Dubourg, J. Vanderplas, A. Passos, D. Cournapeau, M. Brucher, M. Perrot, and E. Duchesnay. Scikit-learn: Machine Learning in Python. *Journal of Machine Learning Research*, 12:2825–2830, 2011.
- Jonas Peters, Dominik Janzing, and Bernhard Schölkopf. *Elements of Causal Inference: Foundations and Learning Algorithms*. Adaptive Computation and Machine Learning series. MIT Press, Cambridge, MA, USA, November 2017. ISBN 978-0-262-03731-0. URL <https://mitpress.mit.edu/9780262037310/elements-of-causal-inference/>.

- Ingo Richter, Ping Chang, Ping-Gin Chiu, Gokhan Danabasoglu, Takeshi Doi, Dietmar Dommenges, Guillaume Gastineau, Zoe E. Gillett, Aixue Hu, Takahito Kataoka, Noel S. Keenlyside, Fred Kucharski, Yuko M. Okumura, Wonsun Park, Malte F. Stuecker, Andréa S. Taschetto, Chunzai Wang, Stephen G. Yeager, and Sang-Wook Yeh. The Tropical Basin Interaction Model Intercomparison Project (TBIMIP). *Geoscientific Model Development*, 18(9):2587–2608, May 2025. ISSN 1991-959X. doi:10.5194/gmd-18-2587-2025. URL <https://gmd.copernicus.org/articles/18/2587/2025/>. Publisher: Copernicus GmbH.
- Jakob Runge, Vladimir Petoukhov, and Jürgen Kurths. Quantifying the Strength and Delay of Climatic Interactions: The Ambiguities of Cross Correlation and a Novel Measure Based on Graphical Models. *Journal of Climate*, 27(2):720–739, January 2014. ISSN 0894-8755, 1520-0442. doi:10.1175/JCLI-D-13-00159.1. URL <http://journals.ametsoc.org/doi/10.1175/JCLI-D-13-00159.1>.
- Jakob Runge, Sebastian Bathiany, Erik Bollt, Gustau Camps-Valls, Dim Coumou, Ethan Deyle, Clark Glymour, Marlene Kretschmer, Miguel D. Mahecha, Jordi Muñoz-Marí, Egbert H. van Nes, Jonas Peters, Rick Quax, Markus Reichstein, Marten Scheffer, Bernhard Schölkopf, Peter Spirtes, George Sugihara, Jie Sun, Kun Zhang, and Jakob Zscheischler. Inferring causation from time series in Earth system sciences. *Nature Communications*, 10(1):2553, December 2019a. ISSN 2041-1723. doi:10.1038/s41467-019-10105-3. URL <http://www.nature.com/articles/s41467-019-10105-3>.
- Jakob Runge, Peer Nowack, Marlene Kretschmer, Seth Flaxman, and Dino Sejdinovic. Detecting and quantifying causal associations in large nonlinear time series datasets. *Science Advances*, 5(11):eaau4996, November 2019b. ISSN 2375-2548. doi:10.1126/sciadv.aau4996. URL <https://www.science.org/doi/10.1126/sciadv.aau4996>.
- Elena Saggioro, Jana de Wiljes, Marlene Kretschmer, and Jakob Runge. Reconstructing regime-dependent causal relationships from observational time series. *Chaos: An Interdisciplinary Journal of Nonlinear Science*, 30(11):113115, November 2020. ISSN 1054-1500, 1089-7682. doi:10.1063/5.0020538. URL <http://arxiv.org/abs/2007.00267>. arXiv:2007.00267 [math, stat].
- Elena Saggioro, Theodore G. Shepherd, and Jeff Knight. Probabilistic causal network modelling of Southern Hemisphere jet sub-seasonal to seasonal predictability. *Journal of Climate*, -1(aop), February 2024. ISSN 0894-8755, 1520-0442. doi:10.1175/JCLI-D-23-0425.1. URL <https://journals.ametsoc.org/view/journals/clim/aop/JCLI-D-23-0425.1/JCLI-D-23-0425.1.xml>. Publisher: American Meteorological Society Section: Journal of Climate.
- N. H. Saji, B. N. Goswami, P. N. Vinayachandran, and T. Yamagata. A dipole mode in the tropical Indian Ocean. *Nature*, 401(6751):360–363, September 1999. ISSN 1476-4687. doi:10.1038/43854. URL <https://www.nature.com/articles/43854>. Publisher: Nature Publishing Group.
- Bernhard Schölkopf, Francesco Locatello, Stefan Bauer, Nan Rosemary Ke, Nal Kalchbrenner, Anirudh Goyal, and Yoshua Bengio. Toward Causal Representation Learning. *Proceedings of the IEEE*, 109(5):612–634, May 2021. ISSN 0018-9219, 1558-2256. doi:10.1109/JPROC.2021.3058954. URL <https://ieeexplore.ieee.org/document/9363924/>.
- Xinwei Shen, Furui Liu, Hanze Dong, Qing Lian, Zhitang Chen, and Tong Zhang. Weakly Supervised Disentangled Generative Causal Representation Learning, August 2022. URL <http://arxiv.org/abs/2010.02637>. arXiv:2010.02637 [cs].
- Fiona R. Spuler, Marlene Kretschmer, Yevgeniya Kovalchuk, Magdalena Alonso Balmaseda, and Theodore G. Shepherd. Identifying probabilistic weather regimes targeted to a local-scale impact variable. *Environmental Data Science*, 3:e25, January 2024a. ISSN 2634-4602. doi:10.1017/eds.2024.29. URL <https://www.cambridge.org/core/journals/environmental-data-science/article/identifying-probabilistic-weather-regimes-targeted-to-a-localscale-impact-variable/DOF1F80FE4ACD2B85F4651FF69F1ED0B>.
- Fiona R. Spuler, Marlene Kretschmer, Magdalena Alonso Balmaseda, Yevgeniya Kovalchuk, and Theodore G. Shepherd. Learning predictable and informative dynamical drivers of extreme precipitation using variational autoencoders. *Weather and Climate Dynamics*, 6(3):995–1014, September 2025. doi:10.5194/wcd-6-995-2025. URL <https://wcd.copernicus.org/articles/6/995/2025/>. Publisher: Copernicus GmbH.
- Fiona Raphaela Spuler, Jakob Benjamin Wessel, Edward Comyn-Platt, James Varndell, and Chiara Cagnazzo. ibicus: a new open-source Python package and comprehensive interface for statistical bias adjustment and evaluation in climate modelling (v1.0.1). *Geoscientific Model Development*, 17(3):1249–1269, February 2024b. ISSN 1991-959X. doi:10.5194/gmd-17-1249-2024. URL <https://gmd.copernicus.org/articles/17/1249/2024/>. Publisher: Copernicus GmbH.
- Cristiana Stan, Cheng Zheng, Edmund Kar-Man Chang, Daniela I. V. Domeisen, Chaim I. Garfinkel, Andrea M. Jenney, Hyemi Kim, Young-Kwon Lim, Hai Lin, Andrew Robertson, Chen Schwartz, Frederic Vitart, Jiabao Wang,

- and Priyanka Yadav. Advances in the Prediction of MJO Teleconnections in the S2S Forecast Systems. June 2022. doi:10.1175/BAMS-D-21-0130.1. URL <https://journals.ametsoc.org/view/journals/bams/103/6/BAMS-D-21-0130.1.xml>. Section: Bulletin of the American Meteorological Society.
- Jessica Steinkopf and Francois Engelbrecht. Verification of ERA5 and ERA-Interim precipitation over Africa at intra-annual and interannual timescales. *Atmospheric Research*, 280:106427, December 2022. ISSN 0169-8095. doi:10.1016/j.atmosres.2022.106427. URL <https://www.sciencedirect.com/science/article/pii/S0169809522004136>.
- Shuangwen Sun, Jian Lan, Yue Fang, Tana, and Xiaoqian Gao. A Triggering Mechanism for the Indian Ocean Dipoles Independent of ENSO. July 2015. doi:10.1175/JCLI-D-14-00580.1. URL <https://journals.ametsoc.org/view/journals/clim/28/13/jcli-d-14-00580.1.xml>. Section: Journal of Climate.
- Maitreyi Swaroop, Eric Elmoznino, and Dhanya Sridhar. Learning Macro Variables with Auto-encoders. 2023.
- Agumase Kindie Tefera, Giovanni Liguori, William Cabos, and Antonio Navarra. Seasonal forecasting of East African short rains. *Scientific Reports*, 15(1):2467, January 2025. ISSN 2045-2322. doi:10.1038/s41598-025-86564-0. URL <https://www.nature.com/articles/s41598-025-86564-0>. Publisher: Nature Publishing Group.
- Axel Timmermann, Soon-Il An, Jong-Seong Kug, Fei-Fei Jin, Wenju Cai, Antonietta Capotondi, Kim M. Cobb, Matthieu Lengaigne, Michael J. McPhaden, Malte F. Stuecker, Karl Stein, Andrew T. Wittenberg, Kyung-Sook Yun, Tobias Bayr, Han-Ching Chen, Yoshimitsu Chikamoto, Boris Dewitte, Dietmar Dommenges, Pamela Grothe, Eric Guilyardi, Yoo-Geun Ham, Michiya Hayashi, Sarah Ineson, Daehyun Kang, Sunyong Kim, WonMoo Kim, June-Yi Lee, Tim Li, Jing-Jia Luo, Shayne McGregor, Yann Planton, Scott Power, Harun Rashid, Hong-Li Ren, Agus Santoso, Ken Takahashi, Alexander Todd, Guomin Wang, Guojian Wang, Ruihuang Xie, Woo-Hyun Yang, Sang-Wook Yeh, Jinho Yoon, Elke Zeller, and Xuebin Zhang. El Niño–Southern Oscillation complexity. *Nature*, 559(7715):535–545, July 2018. ISSN 1476-4687. doi:10.1038/s41586-018-0252-6. URL <https://www.nature.com/articles/s41586-018-0252-6>. Publisher: Nature Publishing Group.
- Arielle S. Tozier de la Poterie, Wasswa Eddie Jjemba, Roop Singh, Erin Coughlan de Perez, Cecilia V. Costella, and Julie Arrighi. Understanding the use of 2015–2016 El Niño forecasts in shaping early humanitarian action in Eastern and Southern Africa. *International Journal of Disaster Risk Reduction*, 30:81–94, September 2018. ISSN 2212-4209. doi:10.1016/j.ijdrr.2018.02.025. URL <https://www.sciencedirect.com/science/article/pii/S2212420918302140>.
- Tomoki Tozuka, Satoru Endo, and Toshio Yamagata. Anomalous Walker circulations associated with two flavors of the Indian Ocean Dipole. *Geophysical Research Letters*, 43(10):5378–5384, 2016. ISSN 1944-8007. doi:10.1002/2016GL068639. URL <https://onlinelibrary.wiley.com/doi/abs/10.1002/2016GL068639>. eprint: <https://agupubs.onlinelibrary.wiley.com/doi/pdf/10.1002/2016GL068639>.
- Caroline M. Wainwright, John H. Marsham, Richard J. Keane, David P. Rowell, Declan L. Finney, Emily Black, and Richard P. Allan. ‘Eastern African Paradox’ rainfall decline due to shorter not less intense Long Rains. *npj Climate and Atmospheric Science*, 2(1):1–9, September 2019. ISSN 2397-3722. doi:10.1038/s41612-019-0091-7. URL <https://www.nature.com/articles/s41612-019-0091-7>. Publisher: Nature Publishing Group.
- Caroline M. Wainwright, Declan L. Finney, Mary Kilavi, Emily Black, and John H. Marsham. Extreme rainfall in East Africa, October 2019–January 2020 and context under future climate change. *Weather*, 76(1):26–31, 2021. ISSN 1477-8696. doi:10.1002/wea.3824. URL <https://onlinelibrary.wiley.com/doi/abs/10.1002/wea.3824>. eprint: <https://rmets.onlinelibrary.wiley.com/doi/pdf/10.1002/wea.3824>.
- Guojian Wang, Wenju Cai, Agus Santoso, Nerilie Abram, Benjamin Ng, Kai Yang, Tao Geng, Takeshi Doi, Yan Du, Takeshi Izumo, Karumuri Ashok, Jianping Li, Tim Li, Sebastian McKenna, Shuangwen Sun, Tomoki Tozuka, Xiaotong Zheng, Yi Liu, Lixin Wu, Fan Jia, Shijian Hu, and Xichen Li. The Indian Ocean Dipole in a warming world. *Nature Reviews Earth & Environment*, 5(8):588–604, August 2024a. ISSN 2662-138X. doi:10.1038/s43017-024-00573-7. URL <https://www.nature.com/articles/s43017-024-00573-7>. Publisher: Nature Publishing Group.
- Kun Wang, Sumanth Varambally, Duncan Watson-Parris, Yi-An Ma, and Rose Yu. Uncovering Latent Causal Structures from Spatiotemporal Data. 2024b.
- Peter J. Webster, Andrew M. Moore, Johannes P. Loschnigg, and Robert R. Leben. Coupled ocean–atmosphere dynamics in the Indian Ocean during 1997–98. *Nature*, 401(6751):356–360, September 1999. ISSN 1476-4687. doi:10.1038/43848. URL <https://www.nature.com/articles/43848>. Publisher: Nature Publishing Group.
- Yinling Zhang, Nan Chen, Jérôme Vialard, and Xianghui Fang. A Physics-Informed Auto-Learning Framework for Developing Stochastic Conceptual Models for ENSO Diversity. November 2024. doi:10.1175/JCLI-D-24-0092.1. URL <https://journals.ametsoc.org/view/journals/clim/37/23/JCLI-D-24-0092.1.xml>. Section: Journal of Climate.

Yiling Zheng, Chi-Yung Tam, and Matthew Collins. Indian Ocean Dipole Impacts on Eastern African Short Rains Across Observations, Historical Simulations and Future Projections. *Earth's Future*, 13(6):e2024EF005219, 2025. ISSN 2328-4277. doi:10.1029/2024EF005219. URL <https://onlinelibrary.wiley.com/doi/abs/10.1029/2024EF005219>. _eprint: <https://agupubs.onlinelibrary.wiley.com/doi/pdf/10.1029/2024EF005219>.